

Transportin-1 binds to the HIV-1 capsid via a nuclear localization signal and triggers uncoating

Juliette Fernandez^{1,7}, Anthony K. Machado^{2,7}, Sébastien Lyonnais³, Célia Chamontin¹, Kathleen Gärtner², Thibaut Léger⁴, Corinne Henriquet⁵, Camille Garcia⁴, Débora M. Portilho², Martine Pugnière⁵, Laurent Chaloin¹, Delphine Muriaux³, Yohei Yamauchi⁶, Mickaël Blaise¹, Sébastien Nisole¹ and Nathalie J. Arhel^{1,2*}

The initial steps of HIV replication in host cells prime the virus for passage through the nuclear pore and drive the establishment of a productive and irreparable infection^{1,2}. The timely release of the viral genome from the capsid—referred to as uncoating—is emerging as a critical parameter for nuclear import, but the triggers and mechanisms that orchestrate these steps are unknown. Here, we identify β -karyopherin Transportin-1 (TRN-1) as a cellular co-factor of HIV-1 infection, which binds to incoming capsids, triggers their uncoating and promotes viral nuclear import. Depletion of TRN-1, which we characterized by mass spectrometry, significantly reduced the early steps of HIV-1 infection in target cells, including primary CD4⁺ T cells. TRN-1 bound directly to capsid nanotubes and induced dramatic structural damage, indicating that TRN-1 is necessary and sufficient for uncoating in vitro. Glycine 89 on the capsid protein, which is positioned within a nuclear localization signal in the cyclophilin A-binding loop, is critical for engaging the hydrophobic pocket of TRN-1 at position W730. In addition, TRN-1 promotes the efficient nuclear import of both viral DNA and capsid protein. Our study suggests that TRN-1 mediates the timely release of the HIV-1 genome from the capsid protein shell and efficient viral nuclear import.

Human immunodeficiency virus (HIV) is released into the host cell cytoplasm as a viral RNA genome encased in a shell of hexagonal arrangements of capsid protein (CA) monomers¹. The capsid is thought to shield the viral genome from cellular innate immune sensors^{3,4} and to create a micro-environment in which the viral reverse transcriptase can convert the RNA genome into double-stranded DNA. It also plays a determining role in the early steps of replication, as it mediates interaction with both the cytoskeleton and nuclear pore complexes (NPC)¹. However, efficient infection ultimately relies on the ability of the viral genome to escape the CA core, which releases the pre-integration complex (PIC) for active transport through the nuclear pore and integration in the host genome. Although it is generally accepted that timely CA shedding is a prerequisite to productive infection¹, the mechanism is unknown.

Given that HIV uncoating is connected to nuclear entry², we reasoned that the cellular proteins that bind to both the CA and karyopherins might be potential co-factors of HIV uncoating and nuclear

import. A previous yeast-two-hybrid screen of the HIV-1 CA performed in our laboratory identified a heterogeneous ribonucleoprotein (hnRNP E1) as a potential CA partner⁵. As many hnRNPs are a cargo of the cellular transport receptor Transportin-1 (TRN-1; gene name, *TNPO1*)⁶, we investigated the role of both hnRNP E1 and TRN-1 on HIV-1 infection. The knockdown of hnRNP E1 did not impact HIV-1 infection but TRN-1 knockdown led to a strong inhibition of infection, implying that it could be a co-factor of HIV uncoating or nuclear import (Extended Data Fig. 1a). TRN-1 is a β -karyopherin (β -Kap) that binds to cargoes in the cytoplasm without adaptors, targets them to the nucleus through the NPC and releases them in the nucleus following RanGTP binding. The experimentally demonstrated and predicted TRN-1 substrates are almost exclusively proteins involved in transcription and RNA processing, with hnRNP A1 being the first and best-characterized example⁶.

Given that other β -Kaps have previously been linked to HIV-1 infection^{7,8}, we tested whether the effect of TRN-1 on HIV might be indirect. First, we showed that TRN-1 depletion was specific and did not disrupt the expression of other β -Kaps (Imp- β 1, Imp-5, Imp-7, Transportin-3 (TRN-SR2 or TRN-3; gene name, *TNPO3*); Extended Data Fig. 1b). Moreover, we noted that TRN-1 knockdown had the strongest impact on HIV-1 infectivity compared with other β -Kaps (Extended Data Fig. 1c). Second, we confirmed that TRN-1 depletion did not significantly reduce cell viability (Extended Data Fig. 1d) or visibly disrupt nuclear pore integrity (Extended Data Fig. 1e). Although TRN-1-knockdown (shTRN-1) cells did proliferate at a slower rate (Extended Data Fig. 1f), this is not expected to impact the nuclear import of lentiviruses such as HIV, which do not require nuclear envelope rupture to access the nucleus⁷. Third, we investigated whether TRN-1 depletion might upset the localization of a host factor important for HIV infection. We used mass spectrometry to analyse molecules with cytosolic accumulation in shTRN-1 cells compared with cells transduced with an empty control (EC) lentiviral vector or depleted for another β -Kap (shImp β -1). The cells were treated with the CRM1-dependent export inhibitor leptomycin B (LMB) before fractionation to enhance the detection of shuttling proteins with short nuclear residency (Extended Data Fig. 2a). Among the proteins that were specifically and significantly enriched in shTRN-1 cytosols (Extended Data Fig. 2b) compared with either the EC or shImp β -1 controls (91 proteins), we found previously

¹Institut de Recherche en Infectiologie de Montpellier, Université de Montpellier, CNRS, Montpellier, France. ²Saint-Louis Hospital, INSERM, Paris 7 University, Paris, France. ³Centre d'Etude des Maladies Infectieuses de Pharmacologie Anti-Infectieuses, CNRS, Université de Montpellier, Montpellier, France. ⁴Plateforme Protéomique Structurale et Fonctionnelle, Institut Jacques Monod, Paris, France. ⁵Institut de Recherche en Cancérologie de Montpellier, INSERM U1194, Université de Montpellier, Institut régional du Cancer de Montpellier, Montpellier, France. ⁶Medical School, University of Bristol, Bristol, UK. ⁷These authors contributed equally: J. Fernandez, A. K. Machado. *e-mail: nathalie.arhel@irim.cnrs.fr

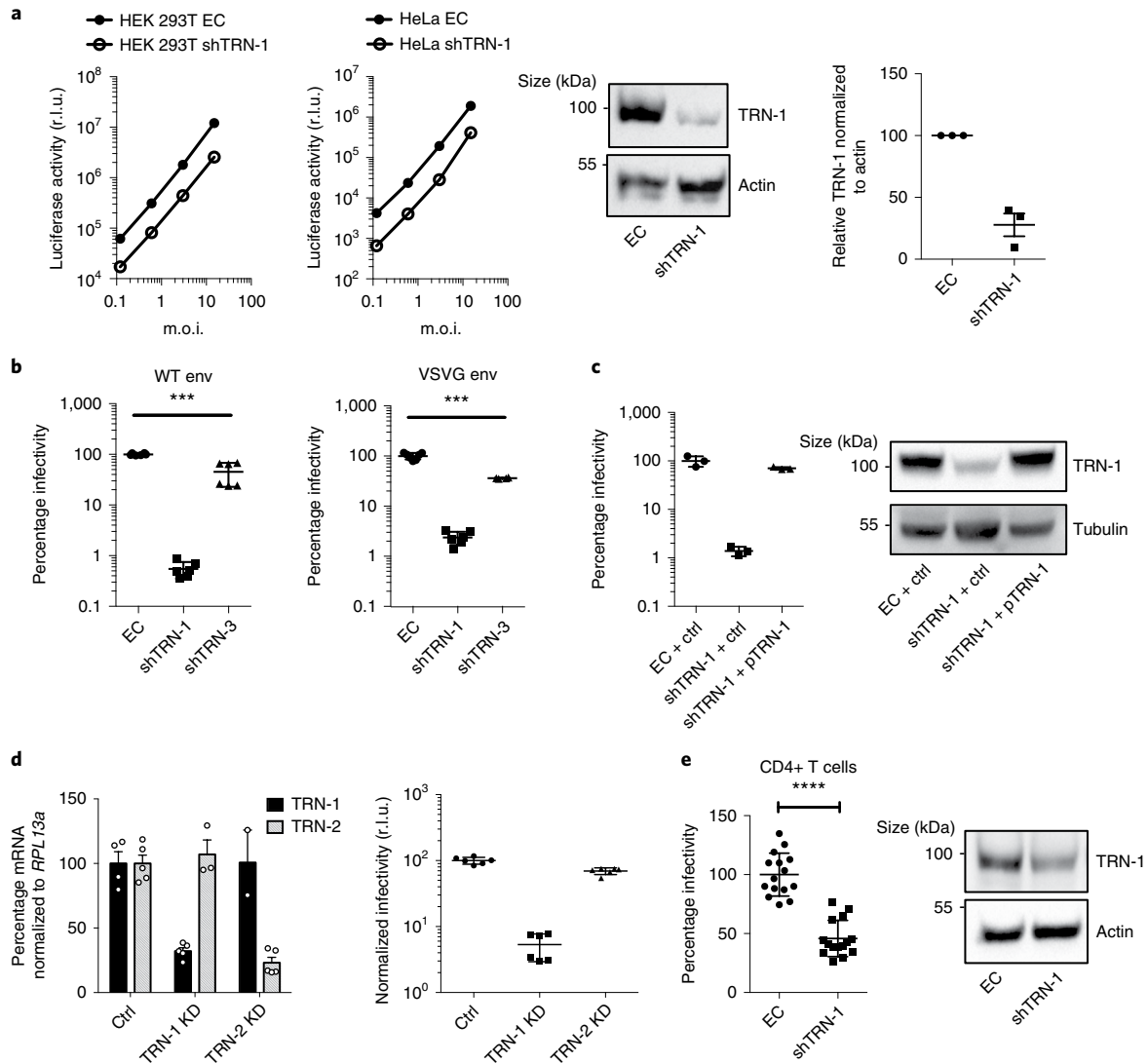


Fig. 1 | TRN-1 promotes the early steps of HIV-1 infection. **a**, TRN-1 promotes HIV-1 transduction. HeLa and HEK 293T cells were transfected with either EC or shTRN-1 vectors and then infected with a CMV-Luc lentiviral vector at the indicated multiplicity of infection (m.o.i.). Luciferase activity was measured at 2 d post infection (d.p.i.; left). The graphs show the mean \pm s.d. ($n=3$ replicates) and are representative of three independent experiments. A representative western blot and the quantification from three independent experiments (mean \pm s.e.m.) show the level of knockdown in HeLa cells (right). r.l.u., relative light units. **b**, TRN-1 promotes HIV-1 infection. P4 TAR- β -gal indicator cells were transfected with the EC, shTRN-1 or shTRN-3 vectors and then infected with HIV-1 (left) or HIV-1-VSVG (right). The β -gal activity was measured at 2 d.p.i. Results show the mean \pm s.d. of three independent experiments performed in triplicate. $***P=0.0002$ and <0.0001 for the WT and VSVG envelope (env), respectively. **c**, TRN-1 is rescued by the add-back of TRN-1. P4 TAR- β -gal indicator cells were transfected with EC or shTRN-1 vectors, transfected with pcDNA3.1 (Ctrl) or pcDNA3.1-HA-TRN-1 (pTRN-1) and then infected with HIV-1-VSVG. The β -gal activity was measured at 2 d.p.i. Results are shown as the mean \pm s.d. ($n=3$ replicates) and are representative of two independent experiments. A representative western blot shows TRN-1 protein levels (right). **d**, HeLa cells were treated with siRNA against TRN-1 or TRN-2 and then infected with a CMV-Luc vector. Knockdown was assessed by qPCR (left) and infectivity by plate luminometry (right). Results show individual values with the mean \pm s.d. from two independent experiments performed in triplicate. KD, knockdown. **e**, Knockdown of TRN-1 reduces HIV-1 infection in primary CD4 $^{+}$ T cells. CD4 $^{+}$ T cells were transfected with EC or shTRN-1 vectors and then infected with HIV-1-GLuc-VSVG. The luciferase activity was measured at 3 d.p.i. Results show the individual values and mean \pm s.d. from three independent experiments (left). $****P<0.0001$. A representative western blot shows the level of TRN-1 knockdown (right).

identified TRN-1 cargoes⁶—such as hnRNP family proteins and ADAR1—but no known cellular interacting partner of the HIV-1 PIC, such as cyclophilin A (CypA), nucleoporins, lens epithelium-derived growth factor (LEDGF/p75) or cleavage and polyadenylation specificity factor (CPSF6; Extended Data Fig. 2c,d). Together, our findings support a direct role for TRN-1 on HIV-1 infection.

Infection by HIV-derived vectors in HeLa and HEK 293T cells (Fig. 1a), and by full-length virus—both wild-type (WT) or vesicular stomatitis virus glycoprotein (VSVG)-pseudotyped HIV-1—in

P4 cells (transactivation response element (TAR)- β -galactosidase (β -gal) indicator cells) was reduced by the knockdown of TRN-1. The knockdown of TRN-3, which has been suggested to promote HIV-1 integration rather than nuclear import^{9–11}, had little effect in this assay (Fig. 1b). The defect in infectivity observed following TRN-1 knockdown was rescued by transfection of TRN-1, thus confirming specificity (Fig. 1c). Moreover, despite 84% identity with TRN-1 (ref. ⁶), Transportin-2 (gene name, *TNPO2*) did not impact HIV-1 infection when depleted (Fig. 1d). Finally, HIV-1 infectivity

was also significantly reduced in CD4+ T cells depleted of TRN-1, confirming that TRN-1 promotes the early steps of infection in natural target cells (Fig. 1e). The dependency of HIV-1 on TRN-1 for infection was observed across different read-outs, with variations in fold effects (from 1.3- to circa 100-fold) depending on the dynamic range of the assay (Extended Data Fig. 3a).

We tested components of the reverse transcription complex for their ability to bind TRN-1 to define how TRN-1 interacts with HIV-1 in cells. No interaction could be demonstrated between haemagglutinin (HA)-TRN-1 and either FLAG-tagged integrase or FLAG-tagged CA following transient transfection (Extended Data Fig. 3b,c). However, CA and TRN-1 were readily co-immunoprecipitated in HIV-1-infected cells (Fig. 2a), suggesting that TRN-1 binds to the incoming cores. Although TRN-1 is predominantly nuclear, endogenous protein was also detected in the cytoplasm and at nuclear pores (Extended Data Fig. 3d), and endogenous TRN-1 colocalized with CA near the nuclear envelope and interacted in proximity ligation assays in infected cells (Fig. 2b and Extended Data Fig. 3e), indicating that TRN-1 can intercept HIV-1 capsids in the cytoplasm and at the nuclear envelope.

TRN-1 binds its substrates via a diverse range of unconventional nuclear localization signals (NLSs) that share only marginal sequence homology to the M9 sequence identified in hnRNP A1 (ref. 12). Some rules have nevertheless been proposed for NLSs that are likely to be recognised by TRN-1 (ref. 13). They typically exist within a stretch of approximately 30 residues that is structurally disordered and overall positively charged with two key regions of contact, a C-terminal PY motif and a central G motif^{8,13,14}. Alignment with the TRN-1-binding motifs of known cargoes, including a recently identified motif in the influenza A virus M1 protein¹⁵, identified a hydrophobic patch in the HIV-1 CA containing a glycine that is critical for recognition by TRN-1 in other known cargoes (highlighted in purple in Fig. 2c)¹³ and downstream basic residues (blue). The glycine at position 89 is in an exposed loop of the HIV-1 CA and is highly conserved across different HIV-1 subtypes¹⁶. Together with the proline at position 90, it is involved in binding to the peptidylprolyl isomerase CypA¹⁷.

We examined the dependency of a G89V mutant virus on TRN-1 to determine the importance of the glycine at position 89 in mediating recognition by TRN-1. We found that the G89V mutant, but not P90A, decreased the dependency on TRN-1 in infectivity assays (Fig. 2d). Although the G89V mutant virus is partly defective for replication (Extended Data Fig. 4a), the loss of dependency on TRN-1 suggested that the glycine at position 89 might be involved in the phenotype. However, binding of CypA at this position is unlikely to play a determining role, given that the P90A mutant (which no longer binds CypA¹⁶) was still dependent on TRN-1 for

infection. None of the other HIV-1 mutants we tested (225T, Q168L and N74D) affected the dependency of HIV-1 on TRN-1 (Extended Data Fig. 4b).

The equivalent glycine (Gly87) in the related but less pathogenic lentivirus HIV-2 is not correctly positioned on the exposed loop, which results in less efficient binding of CypA^{3,18}. We reasoned that this mispositioning could also affect binding to TRN-1 and therefore compared the dependency of HIV-1 and HIV-2 on TRN-1. Unlike HIV-1, we did not observe any significant change in infectivity of HIV-2 following knockdown of TRN-1 (Fig. 2e), confirming that the positioning of the glycine within the exposed loop of the CA is likely to be critical for the TRN-1 recognition of CA. Remarkably, a mutation in HIV-2 (HIV-ac2), which is likely to reposition the glycine in the catalytic site and restore efficient binding to CypA (Extended Data Fig. 4c)³, restored TRN-1 dependency, confirming that the glycine at position 89 on HIV-1 is key in mediating the interaction with TRN-1 (Extended Data Fig. 4d).

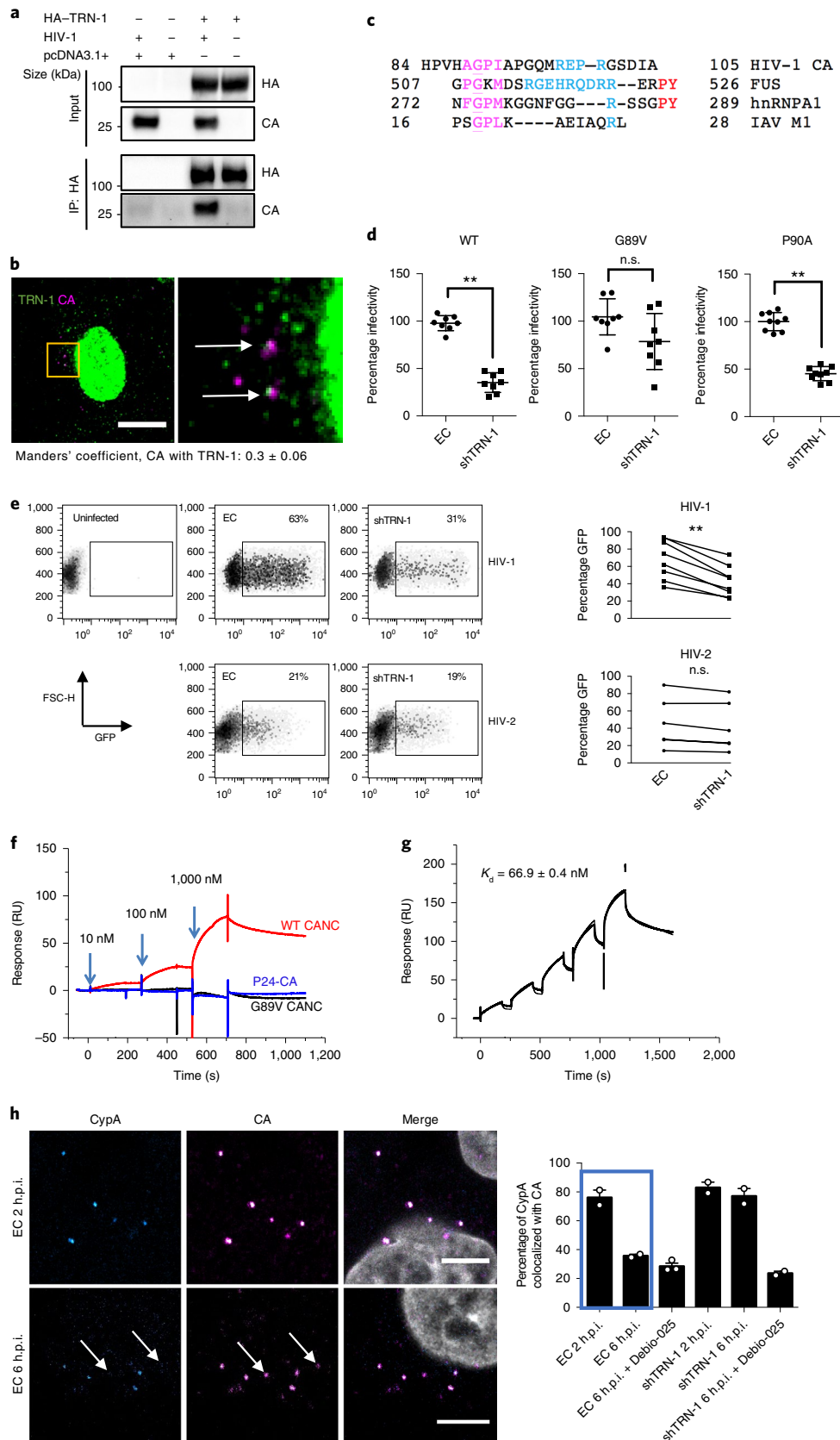
Next, surface plasmon resonance was used to assess whether TRN-1 binds directly to the HIV-1 CA and to confirm that Gly89 mediates recognition. Wild-type and G89V capsid/nucleocapsid (CANC) proteins were produced at high purity, assembled *in vitro* into tubular structures as previously described (Extended Data Fig. 5a)^{19,20} and immobilized on separate flow cells. Unassembled CANC, which forms dimers in solution (Extended Data Fig. 5b), was included as a control. The HIV-1 CANC nanotubes and dimers were incubated with purified recombinant TRN-1 (Extended Data Fig. 5c) or CypA (Extended Data Fig. 5d). In contrast to assembled WT CANC tubes, to which TRN-1 readily bound, no binding was detected between TRN-1 and the G89V CANC tubes or between TRN-1 and the unassembled WT CANC protein (Fig. 2f). The equilibrium dissociation constant (K_d) of TRN-1 for the CANC tubes was estimated to be around 70 nM (Fig. 2g and Extended Data Fig. 5e), compared with 1.5 μ M for CypA with the CANC tubes (Extended Data Fig. 5f), which is concordant with the literature¹⁷.

As CypA and TRN-1 both bind to the CA in a Gly89-dependent manner, and given the higher binding affinity of CA to TRN-1 (2.5 log higher), we reasoned that TRN-1 should displace CypA from CA during infection. To test this, we produced viruses with CypA–DsRed incorporation²¹ and quantified the CA–CypA colocalization at both early and late time points following infection in control and shTRN-1 cells (Fig. 2h). Alternatively, we performed CA pull-down from infected cells and probed for the presence of CypA (Extended Data Fig. 5g). Although CypA colocalization or co-immunoprecipitation with CA decreased with time following the infection of control cells, this effect was lost in cells depleted of TRN-1 (Fig. 2h and Extended Data Fig. 5h). Treatment with the cyclosporin A analogue Debio-025 (ref. 22) displaced CypA from CA

Fig. 2 | TRN-1 binds to assembled HIV-1 CA cores in cells and *in vitro*. **a**, Haemagglutinin immunoprecipitation (IP) at 6 h.p.i. in HEK 293T cells transfected with HA-TRN-1 or empty plasmid, followed by HA and CA western blotting. Images are representative of two independent experiments. **b**, Colocalization analysis of TRN-1 and CA in HeLa cells at 6 h.p.i. on three independent stacks with a total of 713 CA spots (mean \pm s.d.). The arrows indicate points of colocalization. Scale bar, 10 μ m. **c**, Alignment of the HIV-1 CA with known TRN-1 interaction motifs highlighting the following key features: a hydrophobic patch (purple) containing a glycine (underlined), followed by basic residues (blue) and a PY motif (red). IAV M1, influenza A virus M1. FUS, fused in sarcoma protein. **d**, Luciferase activity at 2 d.p.i. in HeLa and HEK 293T cells infected with Luc reporter viruses containing WT (left) or G89V (middle) and P90A (right) mutant capsids. Results show the mean \pm s.d. from three independent experiments performed in triplicate. ** $P=0.0078$ and 0.0039 for WT and P90A, respectively; n.s., $P=0.0781$. **e**, HIV-1 and HIV-2 GFP expression in EC and shTRN-1 HeLa cells at 48 h.p.i. (m.o.i. of 1). Representative flow cytometry results are shown for a single experiment (left) and the graphs show the values from three independent experiments performed at a m.o.i. of 5, 1 and 0.5 (right). ** $P=0.0078$; n.s., $P=0.0625$. **f**, Comparative single-cycle kinetics of TRN-1, injected at 10, 100 and 1000 nM, on assembled WT and G89V CANC tubes, and non-assembled CANC protein immobilized on a CM5 sensor chip performed on a T200 SPR apparatus. Results are representative of three independent experiments. RU, resonance units. **g**, The binding affinity of TRN-1 to HIV-1 nanotubes was assessed by single-cycle kinetic titration of TRN-1 injected at twofold increasing concentrations (62.5–1,000 nM). The thin curve is the fitting curve. This experiment was performed twice with similar results. **h**, Percentage of CypA signal colocalizing with the CA in infected EC or shTRN-1 HeLa cells (right). The mean \pm s.e.m. is shown. Two or more separate image stacks containing a total of 30–40 cells from two independent experiments were analysed for each condition. Cells were treated with 200 nM Debio-025 for 2 h before infection to serve as controls. The images illustrate the first two bars of the graph in the blue box (left). The arrows point to capsids that are CypA negative at 6 h.p.i. Scale bars, 5 μ m.

with the same efficiency that was observed in cells where TRN-1 was present. However, the displacement of CypA did not play a role in the TRN-1 phenotype observed during HIV-1 infection,

given that the dependency on TRN-1 could not be rescued by the knockdown of CypA, treatment with cyclosporin A (Extended Data Fig. 5h) or the P90A CA mutation (Fig. 2d).



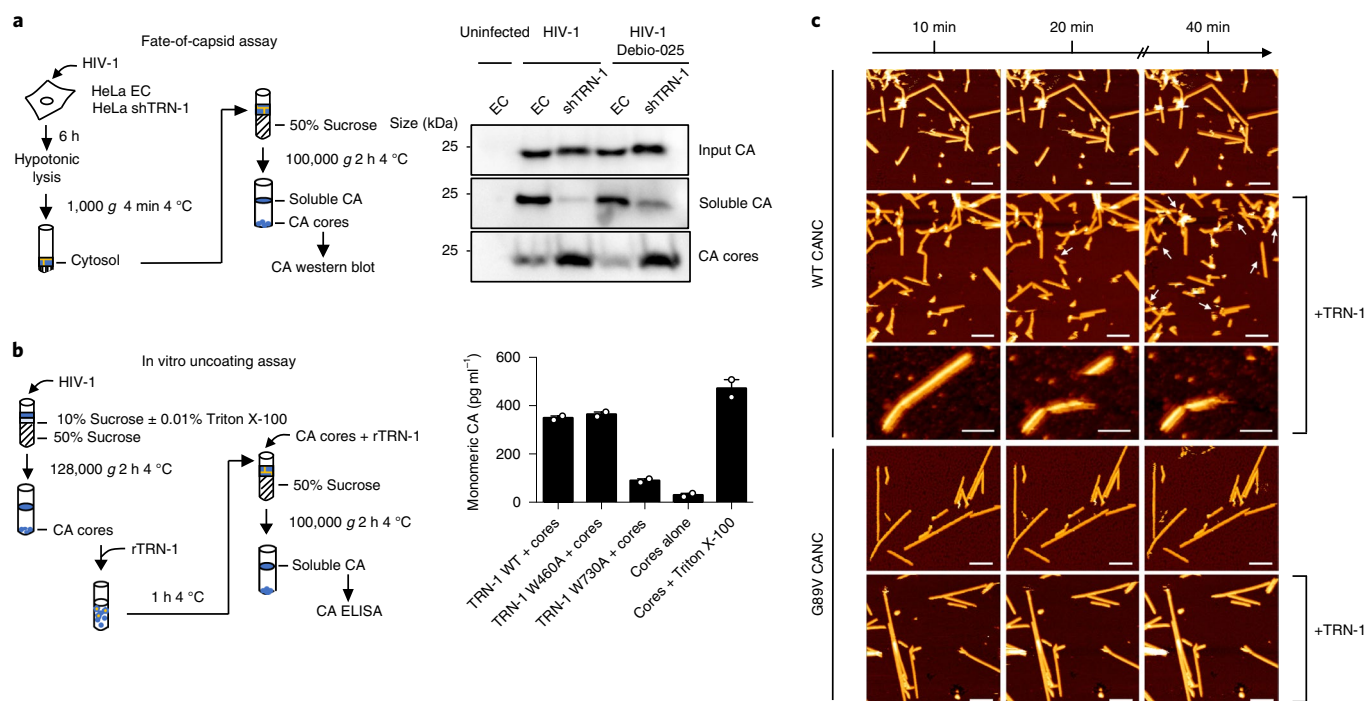


Fig. 3 | TRN-1 triggers HIV-1 uncoating in cells and in vitro. **a**, TRN-1 uncoats HIV-1 in cells. HeLa cells stably transduced with EC or shTRN-1 vectors were infected with VSVG-pseudotyped HIV-1. At 6 h.p.i., soluble CA and still assembled cores were separated by ultracentrifugation on a sucrose cushion and analysed by western blotting of the CA signal (left). The blots are representative of three independent experiments (right). **b**, Recombinant TRN-1 (rTRN-1) uncoats the HIV-1-derived cores and activity maps to W730. HIV-1 CA cores, prepared by ultracentrifugation of HIV-1 virions on a sucrose cushion with 0.01% Triton X-100, were incubated with purified TRN-1 (WT or W460A and W730A mutants) for 1 h at 4 °C and then ultracentrifuged on a sucrose cushion for 2 h at 4 °C to separate the soluble CA (top fraction) from the intact CA cores at the bottom (left). Uncoating was measured by the p24 ELISA quantification of the upper fraction. Results (right) show the individual values from two independent experiments and the mean \pm s.e.m. **c**, Recombinant TRN-1 induces structural damage of CANC tubes assembled in vitro. The WT and G89V self-assembled CANC tubes were adsorbed on a mica surface coated with poly-L-lysine, incubated with recombinant TRN-1 at 20 °C and imaged by atomic force microscopy in buffer. The reaction was followed by recording images every 10 min. The incubation times are indicated. The arrows point to tube breakage, alterations and surface movements. The displayed images are representative of three independent experiments. Scale bars, 500 nm.

Having established that TRN-1 binds to the HIV-1 CA lattices in cells and in vitro, we investigated how this interaction determines the cytoplasmic fate of the incoming cores. First, CA expression and localization was monitored at given time points post infection in the presence of the integrase inhibitor raltegravir to prevent the de novo expression of CA. The CA signal in control cells decreased between 6 and 8 h post infection (h.p.i.), coinciding with uncoating and nuclear import^{21,23}. In contrast, the levels of CA increased in shTRN-1 cells and was readily detected throughout the cytoplasm even at 24 h.p.i., which denoted a failure to shed CA (Extended Data Fig. 6a,b). No cytoplasmic accumulation of CA was observed in shTRN-3 cells (Extended Data Fig. 6b). As β -Kaps have been shown to associate with microtubules²⁴, we questioned whether this defect might reflect an inability of the viral complexes to reach the nuclear envelope, which is a favoured site for uncoating for many viruses^{7,25}. However, quantification of the CA spots present within 0.3 μ m of the nuclear periphery indicated that capsids reached the nuclear envelope by 4 h.p.i. in all samples (41% and 57% of total CA for the EC and shTRN-1 samples, respectively) but that these then scattered back in the cytoplasm in the absence of TRN-1 (Extended Data Fig. 6c).

To address whether TRN-1 promotes HIV-1 uncoating in cells, the stability of viral cores was assessed in cells stably transduced with the EC and shTRN-1 vectors at 6 h following HIV-1 infection using a fate-of-capsid assay. The cytosol of the infected cells was layered onto a sucrose cushion, after which ultracentrifugation yielded soluble CA in the uppermost fraction and CA cores in the

pellet as previously described²⁶ (Fig. 3a). Soluble CA, indicative of full uncoating, was readily detected in the EC-control cytosols but was reduced by $77 \pm 12\%$ (mean \pm s.d.) in cells depleted of TRN-1 (gel imaging analysis from three independent experiments), demonstrating a defect in uncoating in the absence of TRN-1. Treatment with Debio-025, which overrides the inability of capsids to shed CypA in the absence of TRN-1 (Fig. 2h), did not restore efficient uncoating, thus confirming that TRN-1 is required for uncoating irrespective of whether or not CypA is present.

To confirm whether TRN-1 can uncoat HIV-1, we performed in vitro uncoating assays by combining HIV-1 capsids isolated from virions⁵ with recombinant TRN-1 (Extended Data Fig. 6d,e) for 1 h at 4 °C. The degree of CA shedding was assessed by ELISA of the uppermost fraction containing soluble CA after sucrose density ultracentrifugation. The results showed that TRN-1 induced complete uncoating, similar to 5% Triton X-100 (Fig. 3b). TRN-1 makes two essential points of contact with its cognate NLS: with the C-terminal PY motif via a hydrophobic patch that includes residue W460 and with the central GP motif via a hydrophobic pocket formed by W730 (ref. ¹³). We therefore tested the ability of the W460A and W730A mutants to uncoat HIV-1 in vitro. The W460A mutant behaved like the WT TRN-1, whereas uncoating was strongly reduced by the W730A mutation, arguing that this residue is critical for binding to the capsid (Fig. 3b). Therefore, binding of TRN-1 to the CA probably involves interactions between the hydrophobic pocket formed by W730 on TRN-1 and the glycine at position 89 on the CA.

As capsids isolated from virions contain many cellular proteins²⁷, we could not exclude that TRN-1 interacts indirectly with the cores. We therefore assessed the effect of recombinant TRN-1 on assembled CANC over time using atomic force microscopy. The kinetic reaction showed a succession of structural damage to the WT CANC tubes at 20°C within 10 min of the addition of 50 nM TRN-1 protein (Fig. 3c). The tubes mostly underwent structural alterations and sectioning, which resulted in the release of shorter fragments, partial or total desorption and surface movements (Fig. 3c). No such morphological alterations, movements or desorption were observed with the CANC tubes alone or with the G89V mutant tubes incubated with TRN-1, even after a prolonged period of time (75 min) and following an increase of the TRN-1 concentration to 200 nM, demonstrating that TRN-1 strongly destabilizes the structure of the HIV-1 capsid and that the Gly89 residue is critical for recognition by TRN-1. Moreover, these *in vitro* experiments indicate that TRN-1 alone is a major uncoating factor in the absence of other cellular proteins or a reverse transcription reaction.

We performed molecular docking simulations to gain structural insights into the potential binding mode of TRN-1 to the HIV-1 capsid. Rigid docking of TRN-1 on a CA hexamer illustrated how the CypA-binding loop might fit in the TRN-1 pocket—formerly identified to be involved in protein interaction—and notably near the critical Trp730 residue (Fig. 4a–c). According to the docking prediction, TRN-1 may have other points of contact with the CA beside Gly89; in particular, it may insert itself between hexamers, which could induce strong steric hindrance and uncoating.

Although the effect of TRN-1 on HIV-1 uncoating can alone account for the decrease in infection observed in cells depleted of TRN-1 (Fig. 1), its cellular function as a nuclear transporter led us to address whether it could also mediate the nuclear import of HIV-1 after uncoating. We first measured the impact of TRN-1 depletion on HIV-1 reverse transcription and nuclear import by quantifying viral DNA in the nucleus by quantitative PCR (qPCR) amplification of the two long-terminal repeat (2-LTR) junctions and integrated provirus. TRN-1 knockdown did not impair overall levels of viral DNA measured in infected cells but impaired the nuclear accumulation of viral DNA, which may simply confirm that uncoating is a prerequisite for nuclear import (Fig. 4d). The dependency on TRN-1 for HIV-1 infection was maintained in cells arrested in the G1/S phase with aphidicolin, suggesting that TRN-1 favours a nuclear entry pathway that involves passage through the NPC (Extended Data Fig. 7a).

Although capsids are unlikely to pass through NPCs due to their high molecular weight, nuclear CA signal has been detected in infected cells^{28,29} and is proposed to participate in post-nuclear import steps of HIV-1 replication³⁰. We therefore investigated whether TRN-1 can mediate CA transport to the nucleus. Given that TRN-1 binds to cargoes by recognising a NLS, we questioned whether the TRN-1 recognition sequence on the CA is a bona fide NLS. Three different candidate sequences present on the exposed

loop of the HIV-1 CA were tested for their capacity to target glutathione *S*-transferase (GST)–green fluorescent (GFP) fusion proteins to the nucleus. Despite some degree of overlap between sequences, only NLS1 (84-HPVHAGPIAPGQMREPR-100) targeted GST–GFP to the nucleus. Nuclear targeting was exacerbated by the addition of LMB and lost with the G89V NLS1 mutant (Fig. 4e). The CA NLS is present within a disordered loop (residues 80–101; Fig. 4c) and contains other key features of NLSs that bind TRN-1, such as a hydrophobic patch, a central glycine (Gly89) that is critical for binding TRN-1 and downstream basic residues¹³. Although it is devoid of a C-terminal PY motif, similar sequences have been reported for other TRN-1 substrates, such as HuR^{6,31}.

Concordantly, the nuclear CA signal was significantly reduced in cells treated with shTRN-1 compared with the control, indicating that TRN-1 contributes to CA import into the nucleus (Fig. 4f). Furthermore, CA and TRN-1 colocalized at the nuclear envelope and in the nucleoplasm, confirming that TRN-1 could accompany CA into the nucleus (Extended Data Fig. 7b). Interestingly, HIV-1 infection resulted in an overall decrease in cytoplasmic TRN-1, arguing that HIV-1 might usurp cellular TRN-1 for its nuclear import and then prevent its return to the cytoplasm (Extended Data Fig. 7c).

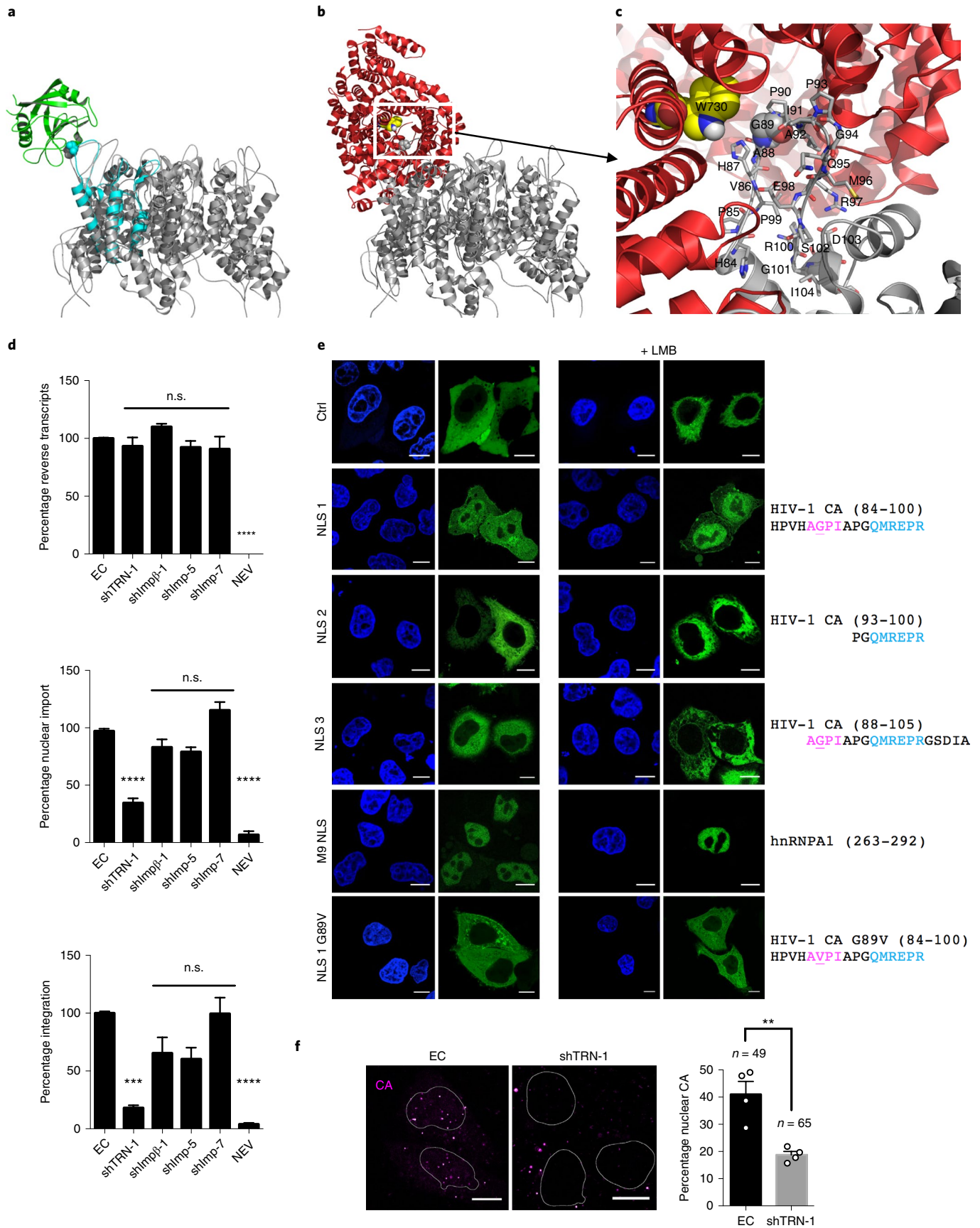
In conclusion, we report that the β -Kap TRN-1 is a co-factor of HIV-1 infection that acts by binding to incoming capsids and triggering their uncoating. The CypA-binding loop of the CA contains a bona fide NLS with a central glycine at position 89 that is critical for engaging TRN-1 at position W730. Although TRN-1 and CypA compete for the same binding site on CA, TRN-1 bound to CANC nanotubes with an apparent dissociation constant of circa 70 nM, which reflects a greater binding affinity than CypA. However, the displacement of CypA from CA by TRN-1 did not account for the effect of TRN-1 on infection.

Binding of TRN-1 to CANC induced immediate and dramatic structural damage to the nanotubes, which probably results in the release of the viral genome in cells. However, although TRN-1 was necessary and sufficient for uncoating *in vitro*, the timing of HIV-1 uncoating is regulated by a number of factors in cells, including the reverse transcription process and binding to cellular co-factors, such as CPSF6, Pin1, CypA and IP6, that regulate the intrinsic stability of the viral core^{32–38}. Intriguingly, the expression levels of TRN-1 did not impact the reverse transcription process—unlike other cellular factors that destabilize the capsid, such as TRIM5 α ³⁹—confirming that the effect of TRN-1 on cores is regulated in cells to promote timely uncoating, which is compatible with productive infection. This may involve cellular factors that shield the capsid from TRN-1 or cellular processes that segregate capsids and TRN-1. For instance, the prevalence of TRN-1 near the nucleus may ensure preferential uncoating of HIV-1 at the nuclear pore, which we observed previously³³. Interestingly, the depletion of microtubular motors or associated proteins

Fig. 4 | Structural insights into the binding of TRN-1 to the CA and the consequences for HIV-1 nuclear import. **a**, Structural simulation of CypA (green) binding to a CA hexamer by superposing the monomeric (Protein Data Base (PDB) accession no. 1M9D; cyan) and hexameric (PDB accession no. 3H4E; grey) structures, for which the Gly89 residues are depicted as spheres. **b**, Rigid docking of TRN-1 (PDB accession no. 4FQ3; red) on a hexameric CA structure (PDB accession no. 3H4E; grey). Trp730 and Gly89 are depicted as yellow and grey spheres, respectively. **c**, Close-up view of the CA loop surrounded by TRN-1. The residues belonging to the loop are labelled and shown as grey sticks (Gly89 is depicted as grey spheres). **d**, TRN-1 promotes the nuclear import of HIV-1 DNA. Reverse transcription efficiency (top), nuclear import (middle) and integration (bottom) were measured by qPCR amplification of the late reverse transcripts, 2-LTR circles and gag–Alu junctions, respectively. The reverse transcriptase inhibitor nevirapine (NEV) was added as a negative control. Results are shown as the mean \pm s.e.m. from six independent experiments performed in triplicate. **** $P < 0.0001$; *** $P = 0.0005$; n.s., non-significant. **e**, The HIV-1 CA contains an NLS sequence. HeLa cells were transfected with different pGST–GFP–NLS plasmids and controls, and treated with/without LMB for 3 h before fixation. Images are representative of two independent experiments. Scale bars, 10 μ m. **f**, TRN-1 promotes the nuclear import of HIV-1 CA. HeLa cells transduced with EC or shTRN-1 vectors were infected with HIV-1–VSVG. The cells were fixed after 6 h and labelled with anti-mouse CA antibody. The CA spots were quantified using Fiji on n nuclei from four separate acquisitions. Scale bars, 10 μ m. Results are shown as the mean \pm s.e.m. ** $P = 0.0039$. Results are representative of two independent experiments.

has been shown to disrupt uncoating, which may reflect their role in trafficking cores to the NPC where uncoating is thought to occur⁴⁰.

After uncoating, TRN-1 transports the HIV-1 CA into the nucleus by recognising its NLS motif. TRN-1 was necessary for the detection of PIC DNA and CA in the nucleus, which could indicate



that TRN-1 transports PICs across the NPCs by dragging on the CA, although further work will be required to functionally separate the effects of TRN-1 on PIC nuclear import and uncoating. Substrates in the nucleus are normally released from TRN-1 by RanGTP binding⁴¹. Here, the fact that CA and TRN-1 still colocalize in nuclei suggests that CA may not be released by nuclear RanGTP. As a result, TRN-1 does not cycle back to the cytoplasm, which may be an additional viral mechanism to ensure that TRN-1 does not trap CAs in the late phases of infection and block virus budding.

Methods

Cells. The following reagents were obtained through the NIH AIDS Reagent Program, Division of AIDS, NIAID, NIH: MT-4 from D. Richman and P4.R5 MAGI from N. Landau. P4 cells are HeLa-based cells that express CD4 and CCR5, and have tat-inducible β -gal activity⁴². HeLa and HEK 293T cells were obtained from the American Type Culture Collection. Citrate human blood was obtained from healthy donors (Etablissement Français du Sang) and peripheral blood mononuclear cells were isolated using Ficoll 100% (Biochrom). CD4+ T lymphocytes were isolated by negative selection with EasySep human CD4+ T cell isolation kit (StemCells), activated by treatment with phytohaemagglutinin (10 μ g ml⁻¹; Fisher Scientific) for 2–3 d and treated with human recombinant IL2 (10 ng ml⁻¹; Immunotools). Cell viability was assessed using an MTT assay. Briefly, 20 μ l MTT solution (5 mg ml⁻¹ thiazolyl blue tetrazolium bromide in PBS; Sigma) was added to the cells. After a 4 h incubation at 37 °C, the medium was replaced with 100 μ l DMSO:EtOH (1:1) solution and placed under agitation for 10 min to lyse the cells. Colorimetry was read at 570 nm with a Tecan plate reader.

Viruses and vectors. The HIV-1 viral molecular clones were based on LAI, LAI Δ env, NL4.3 Δ nefRLuc (*Renilla* luciferase) or NL4.3 Δ nefGLuc (*Gaussia* luciferase). HIV-1-GFP, HIV-2-GFP and HIV-ac2-GFP have been described previously³ and were obtained from N. Manel (Institut Curie). Viruses were produced by transient transfection of HEK 293T cells using calcium-phosphate precipitation with a WT env proviral plasmid or Δ env construct co-transfected with the VSVG envelope expression plasmid pHCMV-G. The vectors used were: HIV-1-eGFP (enhanced GFP), HIV-1-Fluc (Firefly luciferase), HIV-1-NLuc (nanoluciferase) and HIV-2-eGFP⁴³ vectors, as well as short hairpin RNA (shRNA) lentiviral vectors coding for CMV-eGFP and H1-shRNA cassettes within the U3 region. The shRNACypA vector was obtained from J. Luban (University of Massachusetts Medical School). Vectors were produced by transient co-transfection of HEK 293T cells with the vector plasmid, encapsidation (pCMV Δ R 8.74 for HIV-1) and VSVG plasmids. The vectors were harvested after 2 d, filtered and ultracentrifuged at 22,000 r.p.m. for 1 h at 4 °C (SW32Ti rotor). The viruses and vectors were titred by flow cytometry measuring the eGFP expression of HeLa and CHO cells (HIV-1 and HIV-2) or by a p24 (CA) ELISA according to the manufacturer's instructions (Clontech). All shRNA transductions were performed at a m.o.i. of 50 and knockdown was systematically assessed by qPCR for each experiment. Unless otherwise stated, all viral infections were performed at 1 ng p24 per 1,000 cells.

Infectivity assays. Infectivity was assessed by reporter read-out at 48 h.p.i. The levels of β -gal for P4 cells, FLuc and NLuc were measured by plate luminometry, whereas the percentage of eGFP-positive cells was measured by flow cytometry using a FACS Calibur (BD Biosciences). Forward and side scatter were used to gate around the live cell population and eGFP expression was assessed using FlowJo software. Infectivity values in EC cells were set as 100% to plot the mean of several independent experiments.

Antibodies and stains. The primary antibodies used were: mouse monoclonals against β -actin, α -tubulin and FLAG (all from Sigma), p24 (NIH AIDS Reagent program clones 183-H12-5C and AG3.0), integrase (gift from M. Lavigne), TRN-3 (Abcam), lamin A/C (Leica Biosystems), and TRN-1, KPNB1, IPO5 and IPO7 (all from Santa Cruz); rabbit anti-p24 (NIH AIDS Reagent Program SF2), -cyclophilin A (Cell Signaling) and -Nup214 (Abcam); anti-HA from mouse (Sigma), rat (Roche) and rabbit (Abcam). The secondary antibodies were goat anti-mouse and -rabbit (GE Healthcare) or anti-rat (Abcam) horseradish peroxidase conjugates, goat anti-mouse and -rabbit A488 and A647 (Life Technologies). Nuclei were stained with Hoechst dye (Invitrogen).

Drugs. The following drugs were used: Debio-025 (200 nM added for 2 h before infection; Debiopharm), cyclosporin A (2 μ M; Selleckchem), nevirapine (5 μ M; Sigma), raltegravir (10 μ M; Sigma), LMB (50 ng ml⁻¹ for 3 h; Sigma) and aphidicolin (8 μ M; Sigma).

Knockdown experiments. The shRNA sequences were: TRN-1 (NCBI accession no. NM_002270.3), GAGACTATAAGGGAGCCTCT(T); Imp β -1 (NM_002265.6), GCACATGAAAGGATCGACATT; Imp-5 (NM_002271.6), GCTCTAGATCGAATGGCTT(TT); Imp-7 (NM_006391.3),

GATGGAGCCCTGCATATGATT and TRN-3 (NM_012470.3), GGACAGTAACCTTCATGGCT(TT). Short interfering RNAs (siRNAs) against TRN-1 and TRN-2 were ON-TARGETplus SMARTpools from Dharmacon (Horizon Discovery).

Quantitative PCR and RT-PCR. To measure the messenger RNA transcripts, total cellular RNA was isolated using an RNeasy mini kit according to the manufacturer's instructions (Qiagen). PCR with reverse transcription was performed using a One strand synthesis kit (NZY Tech) according to the manufacturer's instructions, and quantifications of complementary DNA were performed using SYBR Green master mix (ROCHE) and normalized to *GAPDH* or *RPL13A*. Specific primer pairs were used to quantify TRN-1 (5'-TTCGAATGGATCGCCTGCTT-3' and 5'-CCGTCCTCGATCGGTGAAAA-3'), TRN-2 (5'-CCTCAACCAGCCGGAATACA-3' and 5'-CGATGACAGACTCCAGCA-3'), Imp β -1 (5'-GTCACAAAACCCCAACAGCAC-3' and 5'-AGCCACTCGTACCCTCGTAT-3'), Imp-5 (5'-TTGCGTCTCACTTGGAAAGC-3' and 5'-AAGTCGCAAGCCATTGAT-3'), Imp-7 (5'-CAGAGGAGCGGAGTCCATTG-3' and 5'-CCCCTTCTTGATTTCCACC-3'), TRN-3 (5'-CAGCTGGAACCAGACCATGA-3' and 5'-GGTGTATCGCACAGCCGTAT-3'), *GAPDH* (NM_002046.6; 5'-GGTGGTCTCTCTGACTTCAACA-3' and 5'-GTTGCTGTAGCCAAATTCGTGT-3'), *RPL13a* (NM_012423.3; 5'-CCTGGAGGAGAAGAGGAAAGAGA-3' and 5'-TTGAGGACCTCTGTATTGTCAA-3') and hnRNP E1 (NM_006196.3; 5'-CAACAGTACCGCGCCAGCA-3' and 5'-ATGGGGGTAGCCACAGCGT-3') mRNAs.

For the late reverse transcripts, 2-LTR and Alu PCR, total cellular DNA was isolated at 24 h.p.i. using the QIAamp DNA micro kit (Qiagen). Circles containing 2-LTRs were detected according to a published protocol⁴⁴ using the pUC-2LTR plasmid, which contains the HIV-1 2-LTR junction, for the standard curve. Reactions were normalized by amplification of the late reverse transcript with the primers MH531/532 and probe LRT-P. The Alu PCR was performed according to a published protocol⁴⁵.

Imaging and analysis. Immunolabelling and proximity ligation assays were performed as previously described⁵. Image stacks were acquired on a LSM 880 confocal (Zeiss) or CODIM super-resolution microscope⁴⁶. Analysis was performed using Imaris and Fiji. Object-based localization was performed using the Fiji plugin JaCoP.

The plasmids expressing different NLS sequences were obtained by cloning the corresponding oligonucleotides flanked with the XbaI and HindIII restriction sites into the pGST-GFP-myc plasmid (Addgene, cat. no. 104451). HeLa cells were transfected for 48 h with 2 μ g of each pGST-GFP-NLS and controls using Fugene6 and subjected to treatment with/without 50 ng ml⁻¹ LMB for 3 h before fixation.

Cell fractionation and LC-MS/MS analyses. P4 cells (1×10^6) were transfected with EC or shTRN-1 vectors in T25 flasks. At 3 d post-transduction, the cells were treated with LMB for 3 h at 37 °C. Cell fractionation was performed on 1×10^6 cells using the NE-PER nuclear and cytoplasmic extraction reagent (Thermo Scientific) following the manufacturer's instructions. The cytoplasmic proteins (30 μ g) were precipitated using methanol/chloroform. The protein pellets were digested overnight at 37 °C with sequencing-grade trypsin (12.5 μ g ml⁻¹; Promega) in 20 μ l of 25 mM NH₄HCO₃. The trypsin-digested peptides were desalted using ZipTip C18 (Merck Millipore). The peptide mixtures were then analysed in triplicate by a Q-Exactive Plus mass spectrometer coupled to a Nano-LC Proxeon 1000 (both from Thermo Scientific). The peptides were separated by chromatography with the following parameters: Acclaim PepMap100 C18 pre-column (2 cm, 75 μ m internal diameter, 3 μ m, 100 Å), Pepmap-RSLC Proxeon C18 column (50 cm, 75 μ m internal diameter, 2 μ m, 100 Å), 300 nL min⁻¹ flow rate, a 98 min gradient from 95% solvent A (water, 0.1% formic acid) to 35% solvent B (100% acetonitrile, 0.1% formic acid). The peptides were analysed in an Orbitrap cell at a resolution of 70,000 with a mass range of m/z = 375–1,500. Fragments were obtained by high collision-induced dissociation activation with a collisional energy of 27%. Tandem mass spectrometry (MS/MS) data were acquired with an Orbitrap cell in a Top20 mode, at a resolution of 17,500. For the identification step, all MS and MS/MS data were processed with the Proteome Discoverer software (Thermo Scientific, version 2.1) and with the Mascot search engine (Matrix Science, version 5.1). The mass tolerance was set to 6 ppm for precursor ions and 0.02 Da for fragments. The following modifications were allowed: oxidation (M), phosphorylation (ST), acetylation (N-ter of protein). The SwissProt database (release date: 02/17) was used with the *Homo sapiens* taxonomy. Peptide identifications were validated using a 1% false-discovery-rate threshold calculated with the Percolator algorithm and then exported to Progenesis QI for Proteomics (version 4.0; Waters) for the relative quantification of their abundances. The relative quantitation was performed using a between-subject analysis and a Hi-3 method, for which the three-most-abundant peptides were used for protein quantitation. Abundance variations of proteins with

at least two unique peptides were considered if their corresponding calculated *P* values were below 0.05.

Immunoprecipitation. HEK 293T cells were seeded in T175 flasks (7×10^6 cells) at day 0, transfected with 60 ng pcDNA3.1+, pHA-TRN and pCA-3×FLAG or pIN-3×FLAG using HEPES and calcium-phosphate precipitation at day 1, and infected or not with LAI-VSVG virus (40 µg p24) at day 2. At 6 or 24 h.p.i., the cells were washed with cold PBS before the addition of crosslinking solution (10 mM DSP in PBS) and incubated for 2 h on ice. Tris (pH 7.5) was then added for 15 min to stop the reaction and the cells were lysed in 10 ml lysis buffer (10 mM Tris pH 7.4, 150 mM NaCl, 1 mM MgCl₂, 1 mM CaCl₂ and 1% Triton X-100) for 30 min at 4 °C.

For capsid immunoprecipitation at different time points, HEK 293T cells were seeded in a petri dish and incubated for 24 h at 37 °C. The cells were transfected with EC or shTRN-1 vectors after changing the medium. The medium was replaced at 48 h post transduction with 5 ml DMEM without FCS, infected with/without LAI-VSVG virus (10 µg p24) and incubated at 37 °C. The cells were trypsinized at 1 h.p.i., washed in PBS before resuspension in DMEM without FCS and further incubated in a Falcon tube on a rocker at 37 °C. At 4 and 8 h.p.i., the cells were washed with PBS and lysed in 10 ml lysis buffer for 30 min at 4 °C.

The lysates were centrifuged for 5 min at 350g and the pellets were resuspended in 2 ml lysis buffer. Complete lysis was performed by three freeze–thaw cycles at –80 °C and the lysates were homogenized with a syringe (18G) before centrifugation at 15,000g for 15 min at 4 °C to pellet the cell debris. A 100 µl volume of supernatant was kept as an input sample and the remaining supernatant was used for CA or HA immunoprecipitation by adding 2 µg of the primary antibody overnight at 4 °C on a wheel. The following day, 50 µl protein G sepharose beads were added to the lysate for 2 h at 4 °C on a wheel, the beads were washed five times in the lysis buffer before elution in 60 µl Laemmli 1×buffer and then vortexed for 15 min. Finally, a 15 min centrifugation at 16,000g was performed to pellet the beads and the supernatant was transferred to a new tube and stored at –80 °C before western blot analysis.

Recombinant protein expression and purification. Haemagglutinin-tagged TRN-1 WT, W460A and W730A cloned into pQE60 (Qiagen) were obtained from M. F. Jantsch (University of Vienna). A tobacco etch virus cleavage site (DIPTTENLYFQG) was added to the N terminus of WT TRN-1 and cloned into pGEX-6P1 for improved purity. Hexahistidine- and GST-tagged TRN-1 were expressed in *Escherichia coli* BL21 (New England Biolabs) transformed with the pRARE2 plasmid. The transformants were cultured at 37 °C in Luria–Bertani medium containing 200 µg ml⁻¹ ampicillin and 30 µg ml⁻¹ chloramphenicol until an optical density at 600 nm of 0.6–1.0 was reached. Protein expression was then induced by the addition of 1 mM isopropyl β-D-1-thiogalactopyranoside and incubated for 4 h at 37 °C. The bacteria were then collected by centrifugation (6,000g at 4 °C for 20 min) and the pellets were resuspended in lysis buffer (50 mM Tris–HCl pH 8, 400 mM NaCl, 5 mM β-mercaptoethanol, 10% glycerol and 1 mM benzamidine). The cells were disrupted by sonication, the lysate was clarified by centrifugation (27,000g at 4 °C for 45 min) and subjected to a first step of GST-Sepharose (GE Healthcare Life Sciences), and the column was washed with three column volumes of a buffer containing 50 mM Tris–HCl pH 8, 1 M NaCl, 5 mM β-mercaptoethanol and 10% glycerol. The protein was then eluted with three column volumes of the following buffer: 50 mM Tris–HCl pH 8, 0.2 M NaCl, 10% glycerol and 20 mM reduced glutathione. The protein was incubated with hexahistidine-tagged tobacco etch virus protease (at a 1:50 (w/w) ratio) with overnight dialysis at 4 °C in 50 mM Tris–HCl pH 8, 0.2 M NaCl, 5 mM β-mercaptoethanol and 10% glycerol. The protein was then subjected to a purification step through immobilized metal affinity chromatography (Ni-NTA Sepharose, GE Healthcare Life Sciences), allowing the cleaved tag and the tobacco etch virus protease to bind to the immobilized metal affinity chromatography column while the cleaved TRN-1 was collected in the flow-through. The protein was then concentrated into Vivaspin20 (50,000 MWCO, Sartorius) and subjected to a size-exclusion chromatography step on a Superdex200 10/300GL column and eluted with the buffer containing 50 mM Tris–HCl pH 8, 0.2 M NaCl, 5 mM β-mercaptoethanol and 10% glycerol. Fractions corresponding to monomeric TRN-1 were collected and concentrated to 2.5 mg ml⁻¹. The purity of the protein was estimated to be 95% when run on a Coomassie blue-stained SDS–PAGE gel.

The WT (from M. H. Malim, King's College London) and G89V CANC, which we generated by site-directed mutagenesis using the GeneArt site-directed mutagenesis system (Thermo Fisher Scientific), were essentially purified as described previously⁴⁷, except that the proteins were loaded on a HiTrap heparin fast-flow column (5 ml; GE Healthcare) and eluted with a linear NaCl gradient. After this purification step by cation exchange, the protein was precipitated using ammonium sulphate and resuspended to about 2.5 mg ml⁻¹ in a buffer containing 30 mM 2-(N-morpholino)ethanesulfonic acid (MES) pH 6 supplemented with 0.5 M NaCl, 1 mM EDTA and 10 mM dithiothreitol before being frozen at –80 °C. The CANC WT and mutant proteins were further purified before performing assembly of the CANC tubes on a size-exclusion chromatography ENrich SEC 650 (BioRad) or Superdex75 10/300GL (GE Healthcare Life Sciences) column and eluted with 50 mM Tris–HCl pH 8 and 100 mM NaCl. Both proteins eluted as a

single and monodisperse peak and the purity of the protein was estimated to be 95% when run on a Coomassie blue-stained SDS–PAGE gel.

Assembly of CANC tubes. In vitro self-assembled CANC tubes were prepared by incubating 40 µM CANC protein with 5 µM TG50 oligonucleotide overnight at room temperature in 50 mM Tris–HCl pH 8.0 and 100 mM NaCl in a total reaction volume of 100 µl.

Surface plasmon resonance. Surface plasmon resonance experiments were performed on a T200 apparatus (GE Healthcare) at 25 °C in running buffer (50 mM Tris pH 7.5, 100 mM NaCl and 0.05% P20). The WT and G89V CANC assembled nanotubes or unassembled CANC were diluted in 10 mM acetate (pH 5) and covalently immobilized (RU levels of 9,000–11,000) on three different flowcells of a CM5S sensor chip by standard amine coupling according to the manufacturer's instructions. A high level of immobilization was required to obtain a binding level of TRN-1 in the range of 100 RU. Kinetic titration experiments (single-cycle kinetics) of recombinant TRN-1 on CAs were performed at a flow rate of 30 µl min⁻¹, first with a tenfold serial dilution (10, 100 and 1,000 nM) and second with twofold serial dilutions (62.5–1,000 nM). The same twofold serial dilutions were used for the affinity determination of CypA.

All curves were evaluated (T200 Evaluation Software 3.0) using a steady-state fitting model for the *K_d* determination of CypA and a heterogeneous fitting model for TRN-1. Only the *K_d* of higher affinity (represented at more than 80% of the total response) was considered for TRN-1. All sensorgrams were corrected by subtracting the low signal from the control reference surface (without any immobilized protein) and buffer blank injections before fitting evaluation. The experiments were repeated two or three times, each time with a new immobilization of assembled CANC nanotubes.

Atomic force microscopy. Capsids purified from HIV-1 virions and in vitro assembled WT HIV-1 CANC and G89V CANC tubes, diluted twofold in buffer A (8.3 µM CANC, 10 mM Tris–HCl pH 7.5 and NaCl 100 mM), were deposited on freshly cleaved mica (Ted Pella, Inc.) coated with 0.01% poly-L-lysine (Sigma) for immobilization and adsorbed for 15 min before imaging. Images were recorded in buffer A using the quantitative imaging mode available on the NanoWizard IV atomic force microscope (JPK Instruments, Bruker). The images were obtained using AC40TS-C2 cantilevers (Olympus) with an applied force kept at 0.15 nN and a constant approach/retract speed of 35 µm s⁻¹ (z range of 50 nm). Buffer A was removed and replaced with buffer A supplemented with 50 nM TRN-1 for kinetic recording. Images were recorded every 10 min at 20 °C.

Transmission electron microscopy. Samples (5 µl) were added to a 200-mesh formvar–carbon grid for 2 min. The grids were stained with 1% uranyl acetate for 1 min. The samples were observed on an Tecnai F20(FEG) microscope.

Fate-of-capsid assay. The HIV-1 core stability in cells was assessed by the separation of soluble CA from CA cores on a sucrose cushion, as described previously²⁶. At 6 h.p.i., the cells were lysed using hypotonic lysis buffer and a dounce homogenizer and briefly centrifuged to clarify the cytosol fractions. The lysates were then layered onto a 50% sucrose cushion and ultracentrifuged at 100,000g for 2 h. The soluble CA (top 100 µl fraction) and intact cores (pellet) were analysed by western blotting of the CA signal.

In vitro CA-uncoupling assay. HIV-1 capsid cores were prepared by centrifuging 500 µl of the viral supernatant on a sucrose cushion (from bottom to top: 1 ml 50% sucrose, 1 ml 10% sucrose + 0.1% Triton X-100 or without Triton X-100 for the negative control) into a 5 ml ultra-clear tube (Beckman, cat. no. 344057) and centrifuged at 32,500 r.p.m. for 2 h at 4 °C (SW55Ti rotor). Following centrifugation, 250 µl soluble CA was taken from the top supernatant, the tube was emptied and the pellet containing the cores was resuspended in 250 µl ice-cold PBS. The capsid cores were then incubated for 1 h on ice with 500 nM of each of the TRN-1 recombinant proteins and ultracentrifuged at 100,000g on 3.5 ml of a 50% sucrose cushion for 2 h at 4 °C in a SW55Ti rotor. After centrifugation, 150 µl soluble CA from the top layer was analysed using a p24 ELISA according to the manufacturer's instructions (Clontech).

Molecular docking. Molecular docking was achieved using the ClusPro v2.0 program⁴⁸ with the crystal structure of CA (PDB accession no. 3H4E) and TRN-1 (PDB accession no. 4FQ3). Before rigid docking, the missing loops and C-terminal tails of each monomer comprising the CA hexamer structure were modelled using the CHARMM program⁴⁹ and CHARMM36 force field⁵⁰. The potential energy of the system was energy minimized by 10,000 steps of steepest descent followed by 50,000 steps of conjugate gradient in explicit water (TIP3P model). The multi-hexamer structure of CA was modelled by fitting the crystal structure of the CA into the cryogenic electron microscopy density map (emd-5136) using Sculptor GUI-based extension of the Situs program v2.8 (ref. ⁵¹) and performing a full exhaustive search in the 6D search space followed by a Powell optimization algorithm for off-lattice refinement. The crystal structures of CypA (PDB accession no. 1M9D) and CA hexamers (PDB accession nos. 3H4E and 5TSX) were used for

overlay and visualization with the PyMOL molecular graphics system (version 1.8, Schrödinger, LLC).

Statistical analysis. All statistical analyses were performed on three independent experiments, or more if otherwise stated, using Prism 6 (GraphPad Software Inc.) software. Statistical significance was determined using a two-tailed Wilcoxon test for Figs. 1e and 2d,e, one-tailed Wilcoxon test for Extended Data Fig. 4d, two-tailed paired *t*-test for Extended Data Figs. 1f and 4b, two-tailed Mann–Whitney test for Extended Data Figs. 5h and 7a, two-tailed unpaired *t*-test for Fig. 4f and Extended Data Figs. 3e, 7c, Kruskal–Wallis test with Dunn's multiple comparison to the EC for Fig. 4d, ordinary one-way analysis of variance for Fig. 1b and Extended Data Fig. 2c, and with multiple comparison to EC control for Extended Data Fig. 1b.

Reporting Summary. Further information on research design is available in the Nature Research Reporting Summary linked to this article.

Data availability

The authors confirm that all relevant data are available on request. The complete LC–MS/MS datasets are available in the PRIDE partner repository⁵² under the identification number [PXD010023](https://www.ebi.ac.uk/pride/archive/study/MSD010023) as raw files, associated pep.xml and xlsx files and label-free report generated by Progenesis Q1.

Received: 22 September 2018; Accepted: 30 August 2019;

Published online: 14 October 2019

References

- Campbell, E. M. & Hope, T. J. HIV-1 capsid: the multifaceted key player in HIV-1 infection. *Nat. Rev. Microbiol.* **13**, 471–483 (2015).
- Ambrose, Z. & Aiken, C. HIV-1 uncoating: connection to nuclear entry and regulation by host proteins. *Virology* **454–455**, 371–379 (2014).
- Lahaye, X. et al. The capsids of HIV-1 and HIV-2 determine immune detection of the viral cDNA by the innate sensor cGAS in dendritic cells. *Immunity* **39**, 1132–1142 (2013).
- Rasaiyaah, J. et al. HIV-1 evades innate immune recognition through specific cofactor recruitment. *Nature* **503**, 402–405 (2013).
- Fernandez, J. et al. Microtubule-associated proteins 1 (MAP1) promote human immunodeficiency virus type I (HIV-1) intracytoplasmic routing to the nucleus. *J. Biol. Chem.* **290**, 4631–4646 (2015).
- Twyffels, L., Gueydan, C. & Kruys, V. Transportin-1 and Transportin-2: protein nuclear import and beyond. *FEBS Lett.* **588**, 1857–1868 (2014).
- Cohen, S., Au, S. & Pante, N. How viruses access the nucleus. *Biochim. Biophys. Acta* **1813**, 1634–1645 (2011).
- Matreyek, K. A. & Engelman, A. Viral and cellular requirements for the nuclear entry of retroviral preintegration nucleoprotein complexes. *Viruses* **5**, 2483–2511 (2013).
- Cribrier, A. et al. Mutations affecting interaction of integrase with TNPO3 do not prevent HIV-1 cDNA nuclear import. *Retrovirology* **8**, 104 (2011).
- Ocwieja, K. E. et al. HIV integration targeting: a pathway involving Transportin-3 and the nuclear pore protein RanBP2. *PLoS Pathog.* **7**, e1001313 (2011).
- Zhou, L. et al. Transportin 3 promotes a nuclear maturation step required for efficient HIV-1 integration. *PLoS Pathog.* **7**, e1002194 (2011).
- Siomi, H. & Dreyfuss, G. A nuclear localization domain in the hnRNP A1 protein. *J. Cell Biol.* **129**, 551–560 (1995).
- Lee, B. J. et al. Rules for nuclear localization sequence recognition by karyopherin β 2. *Cell* **126**, 543–558 (2006).
- Soniat, M. & Chook, Y. M. Karyopherin- β 2 Recognition of a PY-NLS variant that lacks the proline-tyrosine motif. *Structure* **24**, 1802–1809 (2016).
- Miyake, Y. et al. Influenza virus uses transportin 1 for vRNP debundling during cell entry. *Nat. Microbiol.* **4**, 578–586 (2019).
- Gamble, T. R. et al. Crystal structure of human cyclophilin A bound to the amino-terminal domain of HIV-1 capsid. *Cell* **87**, 1285–1294 (1996).
- Yoo, S. et al. Molecular recognition in the HIV-1 capsid/cyclophilin A complex. *J. Mol. Biol.* **269**, 780–795 (1997).
- Price, A. J. et al. Active site remodeling switches HIV specificity of antiretroviral TRIMCyp. *Nat. Struct. Mol. Biol.* **16**, 1036–1042 (2009).
- Campbell, S. & Vogt, V. M. Self-assembly in vitro of purified CA-NC proteins from Rous sarcoma virus and human immunodeficiency virus type 1. *J. Virol.* **69**, 6487–6497 (1995).
- Li, Y. L. et al. Primate TRIM5 proteins form hexagonal nets on HIV-1 capsids. *eLife* **5**, e16269 (2016).
- Francis, A. C., Marin, M., Shi, J., Aiken, C. & Melikyan, G. B. Time-resolved imaging of single HIV-1 uncoating in vitro and in living cells. *PLoS Pathog.* **12**, e1005709 (2016).
- Ptak, R. G. et al. Inhibition of human immunodeficiency virus type 1 replication in human cells by Debio-025, a novel cyclophilin binding agent. *Antimicrob. Agents Chemother.* **52**, 1302–1317 (2008).
- Arhel, N. Revisiting HIV-1 uncoating. *Retrovirology* **7**, 96 (2010).
- Harel, A. & Forbes, D. J. Importin beta: conducting a much larger cellular symphony. *Mol. Cell* **16**, 319–330 (2004).
- Greber, U. F. & Fassati, A. Nuclear import of viral DNA genomes. *Traffic* **4**, 136–143 (2003).
- Yang, Y., Luban, J. & Diaz-Griffero, F. The fate of HIV-1 capsid: a biochemical assay for HIV-1 uncoating. *Methods Mol. Biol.* **1087**, 29–36 (2014).
- Ott, D. E. Cellular proteins detected in HIV-1. *Rev. Med. Virol.* **18**, 159–175 (2008).
- Peng, K. et al. Quantitative microscopy of functional HIV post-entry complexes reveals association of replication with the viral capsid. *eLife* **3**, e04114 (2014).
- Bejarano, D. A. et al. HIV-1 nuclear import in macrophages is regulated by CPSF6-capsid interactions at the nuclear pore complex. *eLife* **8**, e41800 (2019).
- Engelman, A. N. & Singh, P. K. Cellular and molecular mechanisms of HIV-1 integration targeting. *Cell. Mol. Life Sci.* **75**, 2491–2507 (2018).
- Fan, X. C. & Steitz, J. A. Overexpression of HuR, a nuclear-cytoplasmic shuttling protein, increases the in vivo stability of ARE-containing mRNAs. *EMBO J.* **17**, 3448–3460 (1998).
- Rankovic, S., Varadarajan, J., Ramalho, R., Aiken, C. & Rouso, I. Reverse transcription mechanically initiates HIV-1 capsid disassembly. *J. Virol.* **91**, e00289-17 (2017).
- Arhel, N. J. et al. HIV-1 DNA Flap formation promotes uncoating of the pre-integration complex at the nuclear pore. *EMBO J.* **26**, 3025–3037 (2007).
- Hilditch, L. & Towers, G. J. A model for cofactor use during HIV-1 reverse transcription and nuclear entry. *Curr. Opin. Virol.* **4**, 32–36 (2014).
- Marquez, C. L. et al. Kinetics of HIV-1 capsid uncoating revealed by single-molecule analysis. *eLife* **7**, e34772 (2018).
- Mallery, D. L. et al. IP6 is an HIV pocket factor that prevents capsid collapse and promotes DNA synthesis. *eLife* **7**, e35335 (2018).
- Rawle, D. J. & Harrich, D. Toward the “unravelling” of HIV: host cell factors involved in HIV-1 core uncoating. *PLoS Pathog.* **14**, e1007270 (2018).
- Bhargava, A., Lahaye, X. & Manel, N. Let me in: control of HIV nuclear entry at the nuclear envelope. *Cytokine Growth Factor Rev.* **40**, 59–67 (2018).
- Stremelau, M. et al. The cytoplasmic body component TRIM5 α restricts HIV-1 infection in Old World monkeys. *Nature* **427**, 848–853 (2004).
- Dharan, A. & Campbell, E. M. Role of microtubules and microtubule-associated proteins in HIV-1 infection. *J. Virol.* **92**, e00085-18 (2018).
- Chook, Y. M., Jung, A., Rosen, M. K. & Blobel, G. Uncoupling Kap β 2 substrate dissociation and ran binding. *Biochemistry* **41**, 6955–6966 (2002).
- Charneau, P. et al. HIV-1 reverse transcription. A termination step at the center of the genome. *J. Mol. Biol.* **241**, 651–662 (1994).
- Strappe, P. M. et al. Identification of unique reciprocal and non reciprocal cross packaging relationships between HIV-1, HIV-2 and SIV reveals an efficient SIV/HIV-2 lentiviral vector system with highly favourable features for in vivo testing and clinical usage. *Retrovirology* **2**, 55 (2005).
- De Iaco, A. et al. TNPO3 protects HIV-1 replication from CPSF6-mediated capsid stabilization in the host cell cytoplasm. *Retrovirology* **10**, 20 (2013).
- Di Nunzio, F. et al. Human nucleoporins promote HIV-1 docking at the nuclear pore, nuclear import and integration. *PLoS ONE* **7**, e46037 (2012).
- Caron, J. et al. Conical diffraction illumination opens the way for low phototoxicity super-resolution imaging. *Cell Adh. Migr.* **8**, 430–439 (2014).
- Schaller, T. et al. Effects of inner nuclear membrane proteins SUN1/UNC-84A and SUN2/UNC-84B on the early steps of HIV-1 infection. *J. Virol.* **91**, e00463-17 (2017).
- Kozakov, D. et al. The ClusPro web server for protein–protein docking. *Nat. Protoc.* **12**, 255–278 (2017).
- Brooks, B. R. et al. CHARMM: a program for macromolecular energy, minimization, and dynamics calculations. *J. Comp. Chem.* **4**, 187–217 (1983).
- Best, R. B. et al. Optimization of the additive CHARMM all-atom protein force field targeting improved sampling of the backbone ϕ , ψ and side-chain χ_1 and χ_2 dihedral angles. *J. Chem. Theory Comput.* **8**, 3257–3273 (2012).
- Birmanns, S., Rusu, M. & Wriggers, W. Using *Sculptor* and *Situs* for simultaneous assembly of atomic components into low-resolution shapes. *J. Struct. Biol.* **173**, 428–435 (2011).
- Vizcaino, J. A. et al. 2016 update of the PRIDE database and its related tools. *Nucleic Acids Res.* **44**, 11033 (2016).

Acknowledgements

This work was financed by the Labex EpiGenMed, an ‘Investissements d’avenir’ program, reference ANR-10-LABX-12-01, and by the ATIP-Avenir program (2012–2016), Sidaction (2017–2019), ANRS (Agence Nationale de Recherche sur le Sida), CNRS (Centre National de Recherche Scientifique) and the French Ministry of Higher Education and Research. The atomic force microscopy was financed by the REDSAIM project—Pacte métropolitain d’innovation de Montpellier. We thank the proteomics platform of the Institut Jacques Monod (UMR7592, Paris Diderot University, CNRS) for performing the mass spectrometry, A. Neyret (CEMIPAI) and the Electron Microscopy Platform (COMET) of the Institute for Neurosciences of Montpellier for the electron microscopy, A. Hance (formerly Inserm U941, Hôpital Saint-Louis) for helpful discussions about the project and K. Ford-Powell for critical reading of the manuscript.

Author contributions

J.F., A.K.M., S.L., C.C., D.M.P., M.B., S.N. and N.J.A. performed the experiments. T.L., C.G. and L.C. performed the proteomic and structural data analyses. C.H. and M.P. performed the surface plasmon resonance analysis. K.G., D.M. and Y.Y. provided conceptual input. N.J.A. wrote the manuscript with input from all of the authors.

Competing interests

The authors declare no competing interests.

Additional information

Extended data is available for this paper at <https://doi.org/10.1038/s41564-019-0575-6>.

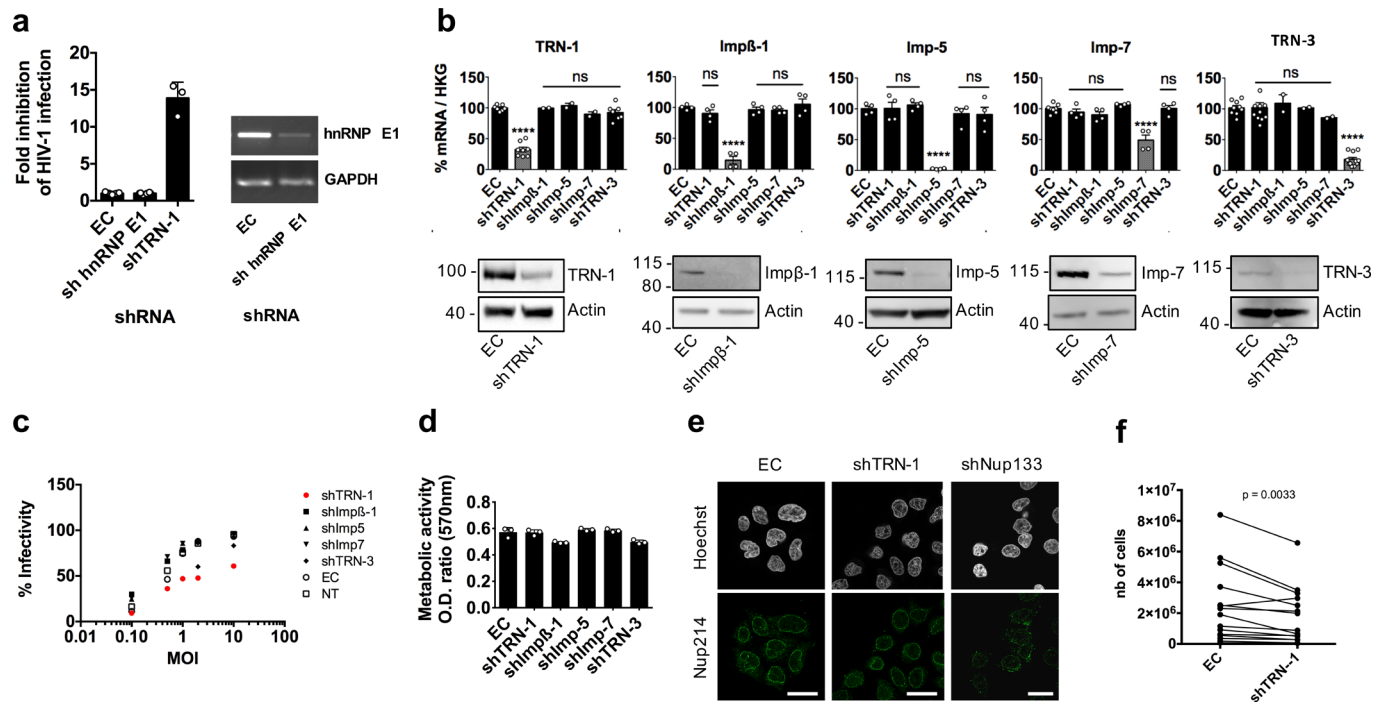
Supplementary information is available for this paper at <https://doi.org/10.1038/s41564-019-0575-6>.

Correspondence and requests for materials should be addressed to N.J.A.

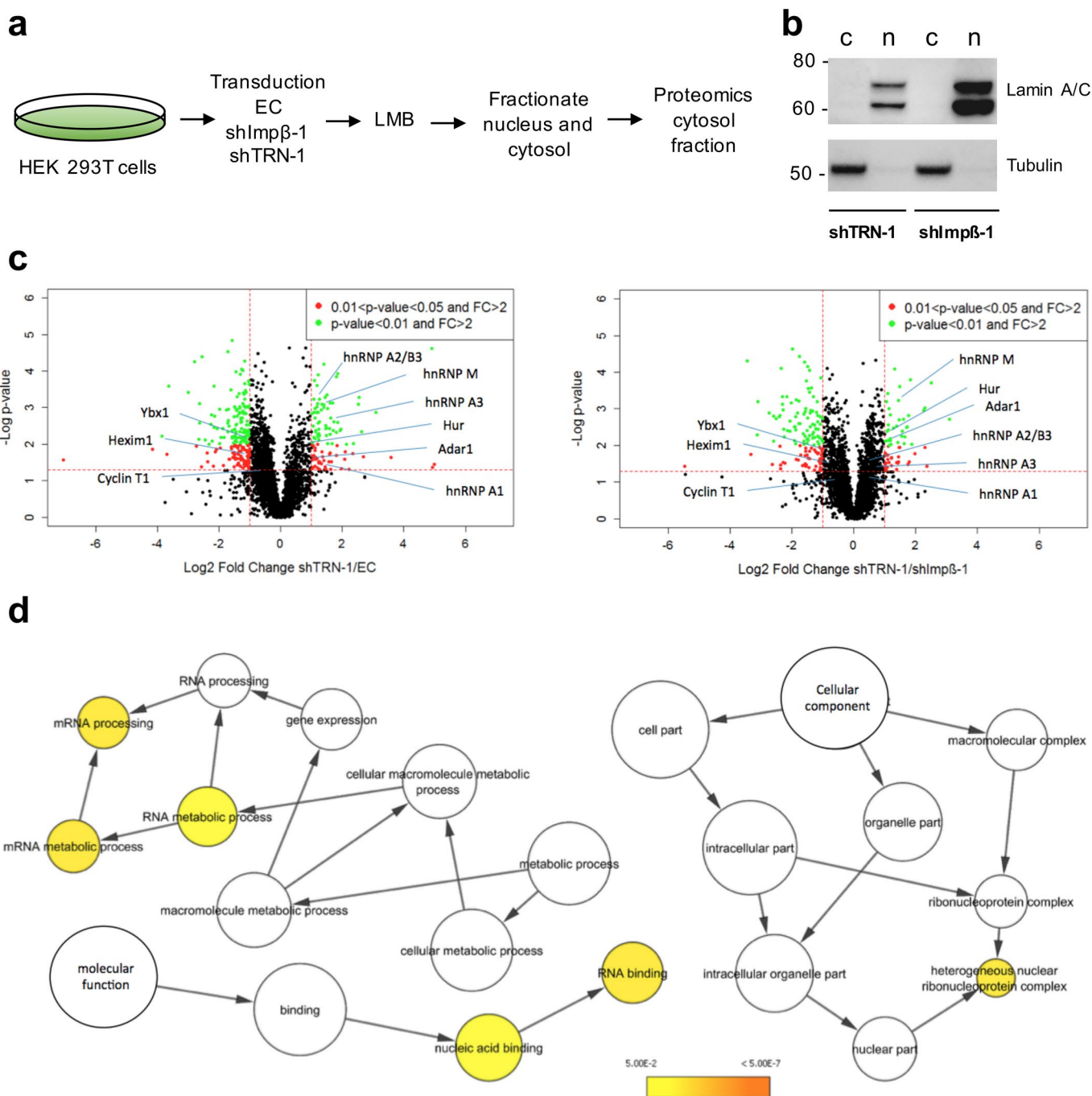
Reprints and permissions information is available at www.nature.com/reprints.

Publisher's note Springer Nature remains neutral with regard to jurisdictional claims in published maps and institutional affiliations.

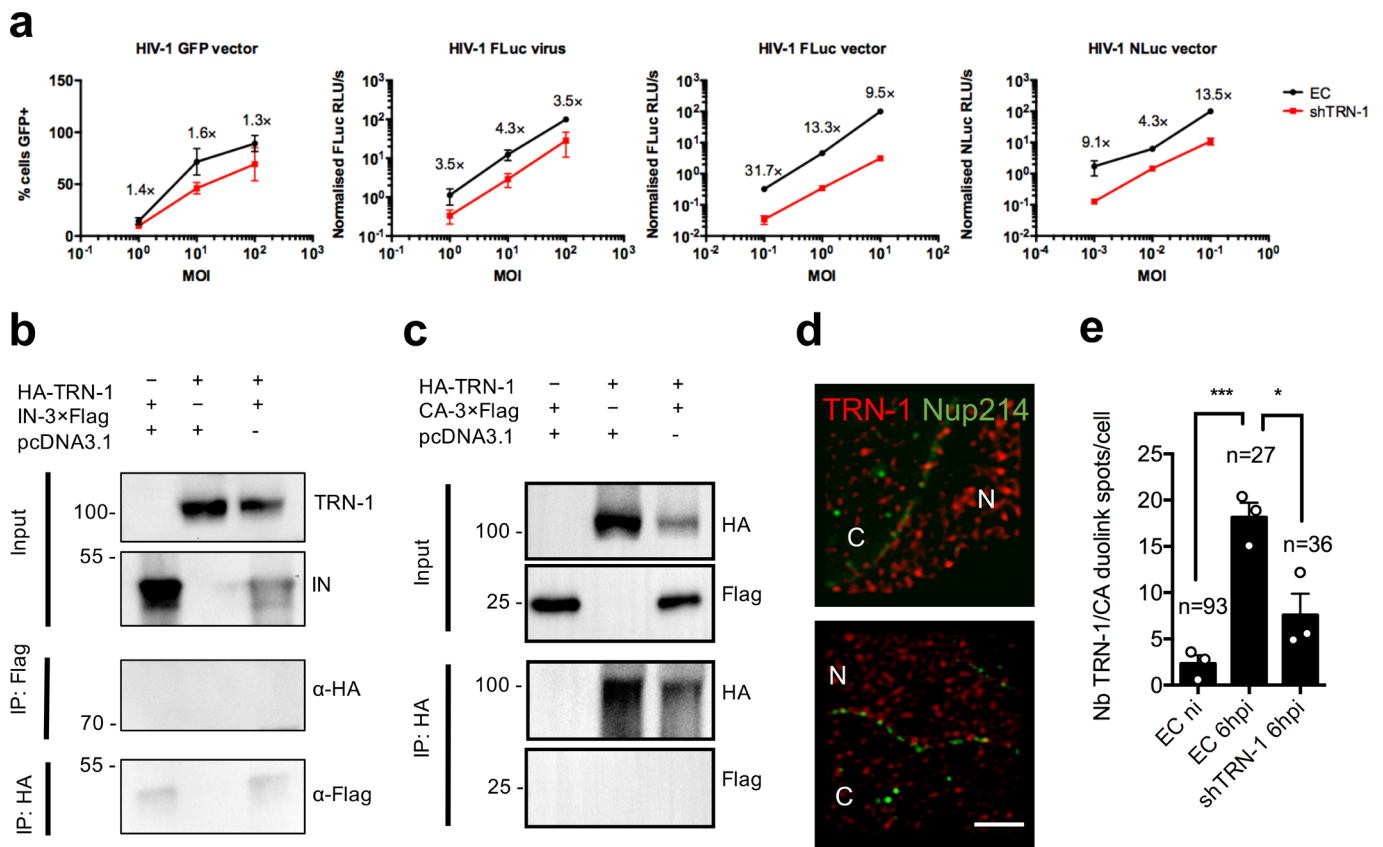
© The Author(s), under exclusive licence to Springer Nature Limited 2019



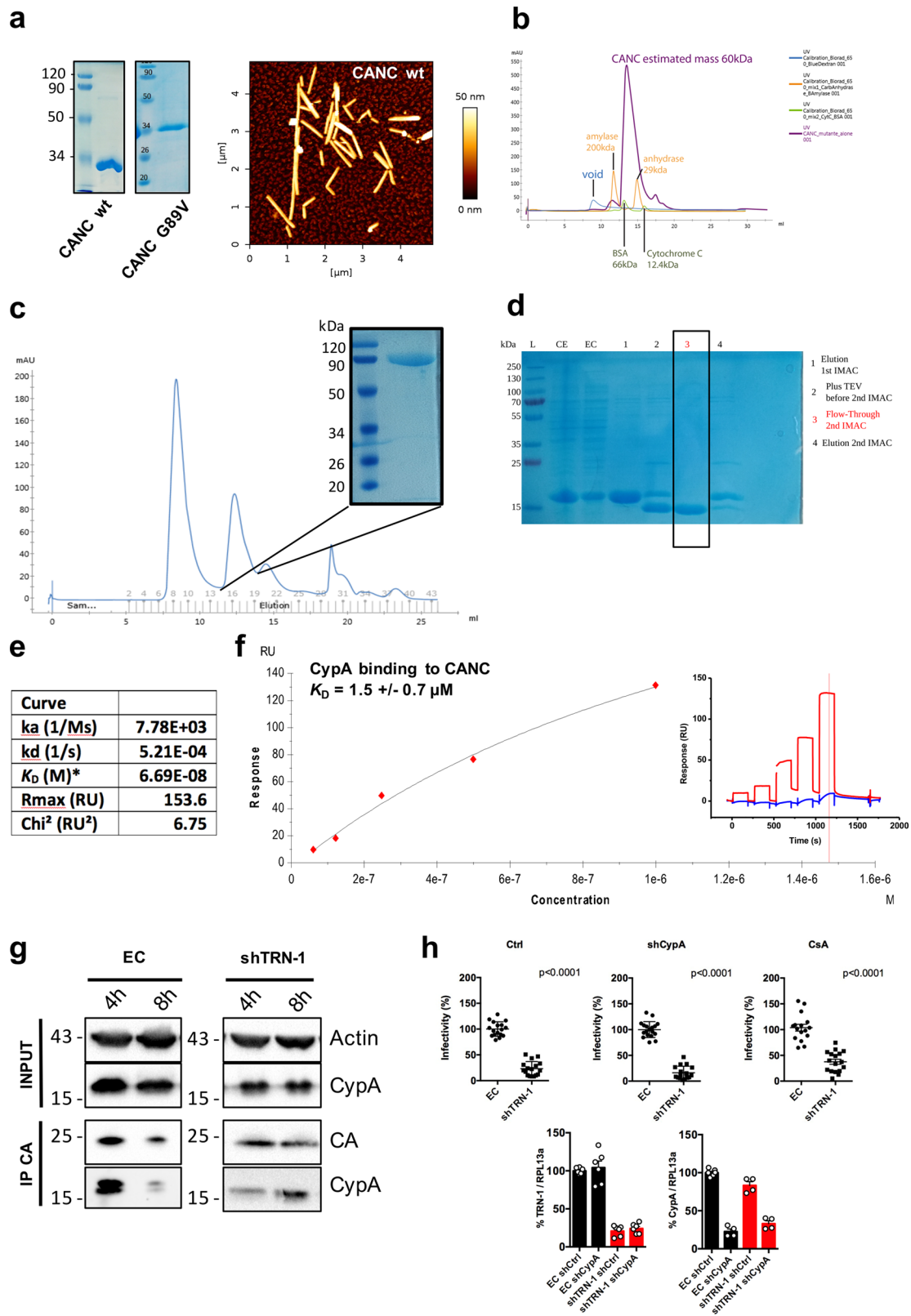
Extended Data Fig. 1 | Comparative profiling of TRN-1 knockdown cells. **a**, Inhibition of HIV-1 infection by TRN-1 knockdown. P4 TAR- β -gal indicator cells were transduced with EC, shhnRNP E1 or shTRN-1, then infected with VSVG pseudotyped HIV-1. β -gal activity was measured at 2 d.p.i. Results show mean \pm s.d. of multiple replicates from 2 independent experiments. Gels show hnRNP E1 and GAPDH transcript levels following RT-PCR. TRN-1 knockdown is shown in panel **b**. **b**, Kap knockdown is specific. HeLa or HEK 293T cells were transduced with the indicated shRNA lentiviral vectors at m.o.i. 50. Results show the mean of triplicates \pm s.e.m. from 3 independent experiments. qPCR results were normalized for housekeeping (HKG) gene transcripts GAPDH or RPL13a. **** $p < 0.0001$, ns = non-significant. Representative western blots from HeLa cells are shown below. **c**, Effect of Kap knockdown on HIV-1. HeLa cells were treated with specific shRNAs, EC, or not treated (NT), then transduced with a HIV-1-eGFP vector at the indicated m.o.i.s. Infectivity was assessed at 48 hpt by flow cytometry analysis. Results show individual values from 2 independent experiments. **d**, Kap knockdown does not compromise cell viability. Cell viability was measured by MTT assay at 3 dpt on HeLa cells transduced with the indicated shRNAs. Data show the mean of triplicate samples \pm s.d. and are representative of 3 independent experiments. **e**, TRN-1 knockdown does not disrupt nuclear pore integrity. Nup214 localization was assessed by confocal fluorescence microscopy in cells treated with EC control, or specific shRNAs against TRN-1 or Nup133, the latter of which was previously shown to disrupt nuclear pore formation⁴⁹. Images are representative of 2 independent experiments. Scale bar = 10 μ m. **f**, TRN-1 knockdown cells have a slower proliferation rate. An equal number of HeLa cells treated with either shTRN-1 or EC were counted at 3 dpt. Paired t test was performed on $n = 16$ independent knockdown experiments.



Extended Data Fig. 2 | Proteomic characterization of TRN-1 knockdown cells. **a**, Proteomic screen of cells depleted of TRN-1. Flowchart of the methodology used to identify proteins that accumulate in the cytosol of TRN-1 knockdown cells. **b**, The quality of the cytoplasmic (c) and nuclear (n) fractions that were used for mass spectrometry was assessed by western blotting. **c**, Volcano plot of quantitative mass spectrometry analysis using protein abundance ratios from the shTRN-1 condition compared to the EC (left) and shImpβ-1 (right) conditions. Peptides mixtures were analysed in triplicate. The dashed lines correspond to p-values and Fold Change thresholds of respectively 0.05 and 2. The entire datasets are available from the Pride repository. **d**, Gene ontology term enrichment analyses of proteins whose abundances are increased in the shTRN-1 condition compared to EC and shImpβ-1 conditions. Differential terms (corrected p-value > 0.01, Benjamini and Hochberg correction) given by BINGO module and Cytoscape software are represented in yellow.

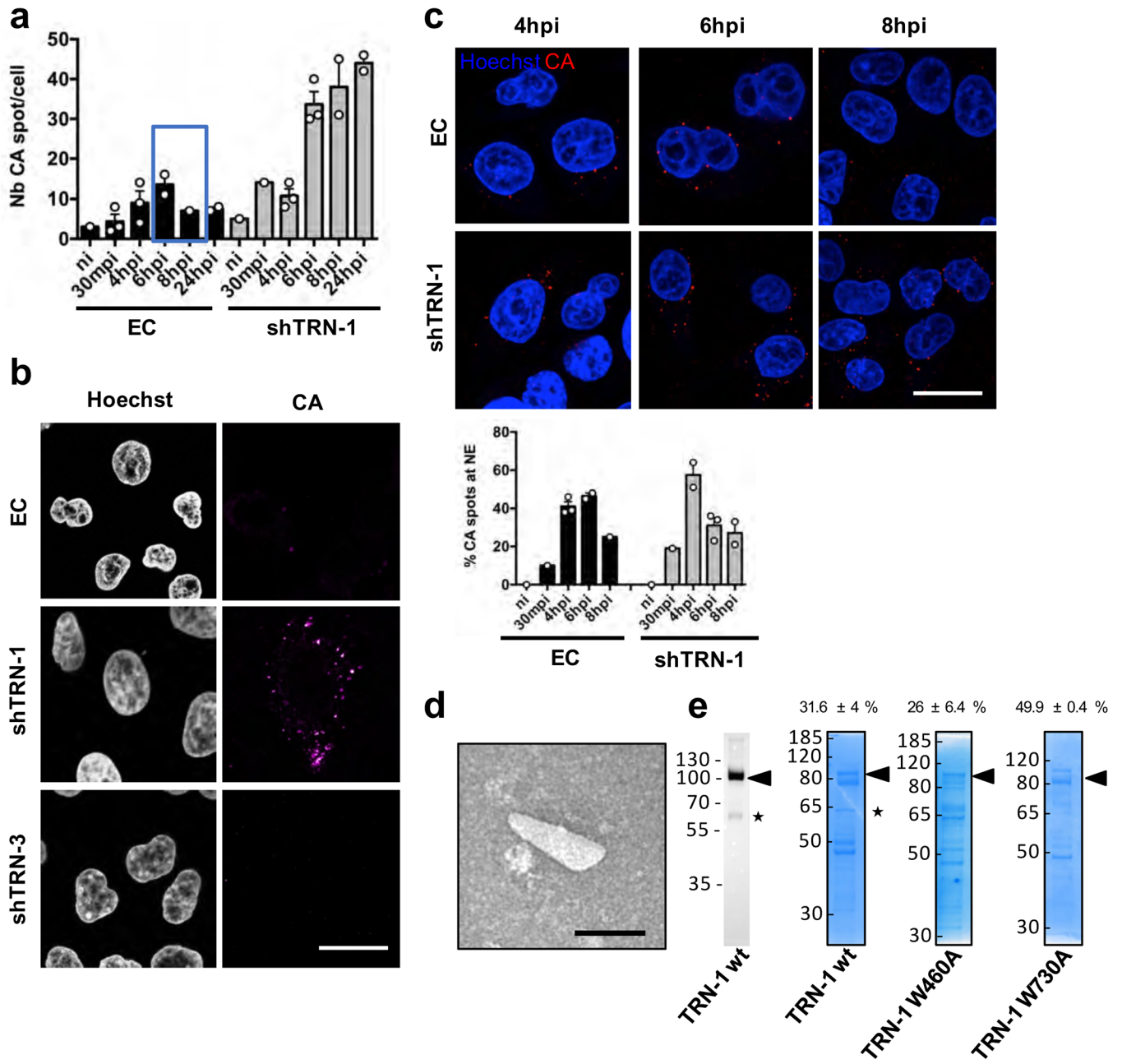


Extended Data Fig. 3 | Characterization of the dependency of HIV-1 infection on TRN-1. **a**, HeLa cells depleted of TRN-1 were infected with different HIV-1 reporter viruses or vectors. Infectivity was measured by the percentage of GFP positive cells (flow cytometry) or the luciferase activity (luminescence) at 48 h.p.i. Results show the mean of 3 independent experiments performed in triplicate \pm s.d. Numbers indicate the average fold changes between EC and shTRN-1 samples across 3 independent experiments. **b**, TRN-1 does not bind HIV-1 integrase. HEK 293T cells were co-transfected with HA-TRN-1, IN-3xFLAG, or empty plasmid pcDNA3.1+. After 24 h, HA or FLAG immunoprecipitation was performed, followed by HA and FLAG western blotting. Blots are representative of 3 independent experiments. **c**, TRN-1 does not interact with ectopically expressed CA. HEK 293T cells were co-transfected with HA-TRN-1, CA-3xFLAG, or empty plasmid pcDNA3.1+. After 24 h, HA immunoprecipitation was performed, followed by HA- and FLAG- western blotting. The blots are representative of two independent experiments. **d**, TRN-1 endogenous localization in uninfected cells. HeLa cells were labelled with mouse anti-TRN-1 and rabbit anti-Nup214 antibodies. Images were acquired with a CODIM super-resolution microscope and are representative of 3 independent experiments. C=cytoplasm, N=nucleus. Scale bar = 2 μ m. **e**, TRN-1 and CA co-localize in infected cells. EC or shTRN-1 transduced HeLa cells were infected with HIV-1-VSVG or left uninfected. Duolink labelling was performed at 6 h.p.i. using anti-rabbit TRN-1 and anti-mouse p24. Image analysis was performed in 3D with Imaris on *n* cells from 3 separate acquisitions (mean values \pm s.e.m.). *** $p=0.001$, * $p=0.198$. Results are representative of 2 independent experiments.



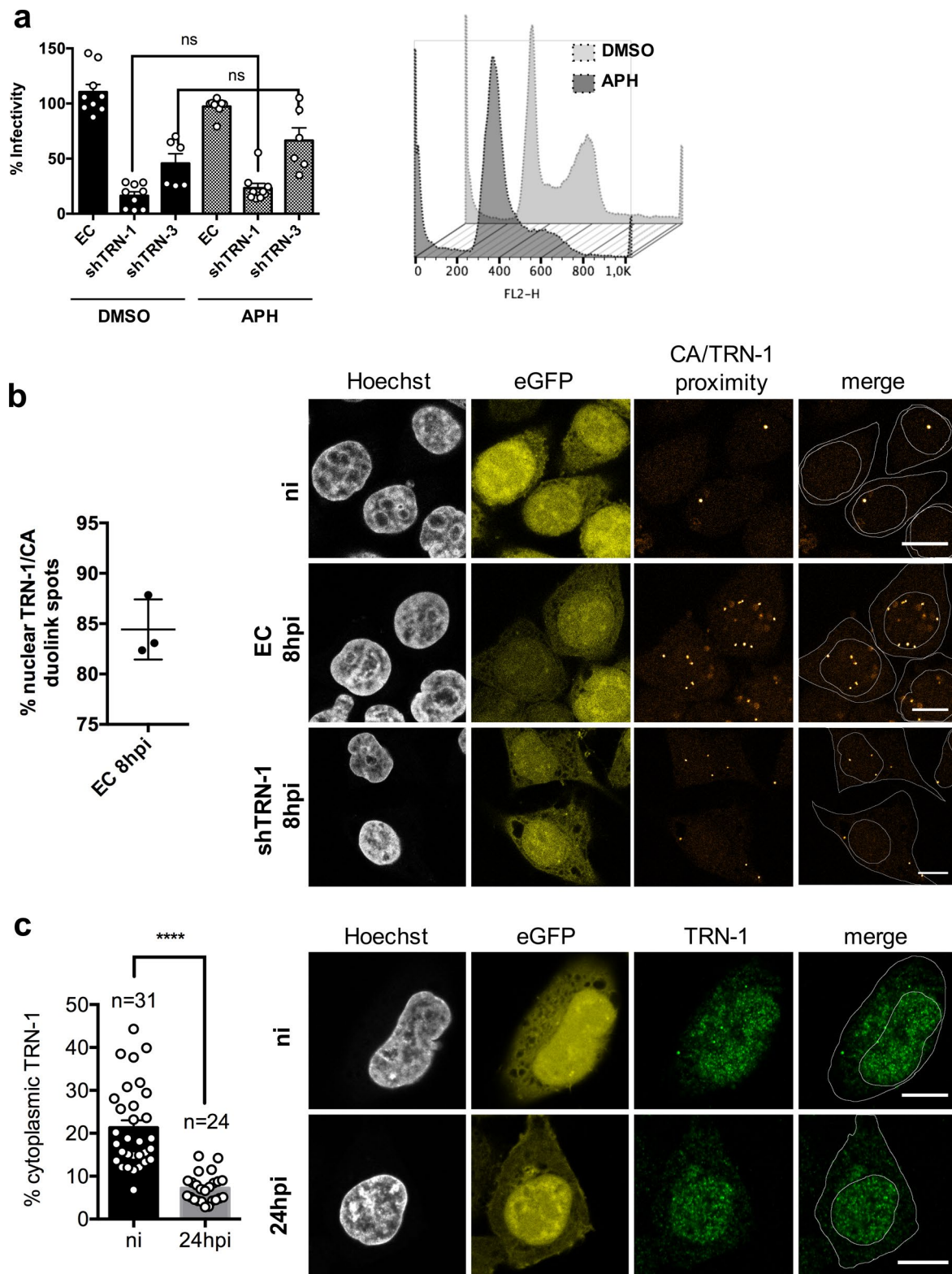
Extended Data Fig. 5 | see figure caption on next page.

Extended Data Fig. 5 | Recombinant proteins and *in vitro* binding assays. **a**, Coomassie gels of the recombinant CANC and CANC-G89V preparations that were used for the *in vitro* experiments. The AFM image is representative of 5 independent preparations of *in vitro* assembled CANC tubes. **b**, The oligomeric state of CANC in solution was assessed on an ENrich SEC 650 gel-filtration column (Bio-Rad) eluted with 50 mM Tris-HCl pH 8, 100 mM NaCl, at a flow rate of 0.4 ml min⁻¹ at 4 °C. The molecular weight was determined based on a calibration curve obtained using the Gel Filtration Markers Kit for Protein Molecular Weights of 12,400–200,000 Da (Sigma-Aldrich) and dextran blue to assess the column void volume. The apparent mass of CANC was obtained by plotting the partition coefficient K_{av} against the logarithms of the molecular weights of standard proteins. We estimated this mass to about 60kDa, which is almost two times the theoretical mass of CANC (33kDa). This experiment was repeated twice with similar results. **c**, Purification of the recombinant TRN-1 stock that was used for Fig. 2f, g and ED Fig. 5e. TRN-1 purification on size-exclusion chromatography Superdex 200 increase 10/300 GL and Coomassie Blue Stained SDS-PAGE of pooled fractions of the SEC column (10 µg of protein loaded on gel). The elution peak corresponds to a monomer (100kDa) and the purity of the protein was estimated to be 95%. **d**, Coomassie gel of the purified CypA preparation that was used for *in vitro* experiments. Flow-through from second IMAC shown in lane 3 was used for SPR experiments. **e**, Kinetic data table obtained from the sensorgram of Fig. 2g using a heterogeneous fitting model. Only the equilibrium constant K_D of higher affinity (more than 80% of the total response) is given, k_a and k_d are rate association and dissociation constants respectively, R_{max} the maximum analyte binding capacity, and χ^2 is a measure of the average squared residual (the difference between the experimental data and the fitted curve). This experiment was performed twice with similar results. **f**, Determination of CypA affinity on WT CANC: SPR fitting curve using steady-state model evaluated from a single cycle kinetic titration of CypA injected at increasing concentrations from 62.5 to 1000 nM on immobilized WT CANC (inset, red curve). Comparatively titration curve of CypA on G89V CANC immobilized (inset, blue). The estimated K_D is provided +/- SE. This experiment was performed twice with similar results. **g**, TRN-1 favours CypA removal from HIV-1 CA. HeLa cells transduced with EC or shTRN-1 were infected with HIV-1-VSVG. Cells were lysed at 4 and 8 h.p.i., capsids were immunoprecipitated and probed with anti-CypA antibody. Results are representative of two independent experiments. **h**, CypA removal from CA does not rescue dependency of HIV-1 on TRN-1. EC and shTRN-1 HeLa and HEK 293T cells were transduced with shCypA or control vector, or treated with 2 µM Cyclosporin A (CsA), then infected with HIV-1-FLuc virus. Results were normalized for infection in EC cells for each condition. Top graphs show the mean +/- SD of 3 independent experiments, each carried out at different m.o.i. in triplicate. **** $p < 0.0001$. Bottom graphs show the qPCR quantification of TRN-1 and CypA transcripts.



Extended Data Fig. 6 | see figure caption on next page.

Extended Data Fig. 6 | Characterization of the uncoating of HIV-1 by TRN-1. **a**, TRN-1 depletion causes HIV-1 capsid to persist in the cytoplasm of infected cells. HeLa cells transduced with EC or shTRN-1 were infected with VSVG-pseudotyped HIV-1 in the presence of Raltegravir. Cells were fixed at the indicated times points post-infection. Viral capsid was immunolabelled and 2-4 image stacks were acquired by LSM880 confocal microscope for each time point. CA spots were quantified in 3D using Imaris and are shown as the mean \pm s.e.m. from one experiment, representative of 3 independent experiments. **b**, TRN-3 depletion does not prevent HIV-1 uncoating. HeLa cells were transduced with shTRN-1 or shTRN-3, then infected with VSVG pseudotyped HIV-1 in the presence of raltegravir. Images show CA labelling in a representative field at 24 h.p.i. Scale bar = 10 μ M. Results are representative of two independent experiments. **c**, Knockdown of TRN-1 does not impede incoming viral trafficking. HeLa cells transduced with EC or shTRN-1 were infected with VSV-G pseudotyped HIV-1 and fixed at the indicated time points post-infection. Viral capsid was immunolabelled and 2-4 image stacks were acquired by LSM880 confocal microscope for each time point. The nuclear volume and CA spots within 0.3 μ m distance of the nuclear envelope were detected in 3D using Imaris and are shown as the mean \pm s.e.m. from one experiment, representative of 2 independent experiments. Scale bar = 10 μ M. **d**, TEM image of a representative capsid isolated from HIV-1 virions on sucrose cushion, used in Fig. 3b. Scale bar = 100 nm. Results are representative of two independent experiments. **e**, Coomassie gels of recombinant TRN-1 enrichment used for Fig. 3b. TRN-1 appears as a 102 kDa band (arrows). Quantification is provided at the top of each lane. Other bands may be degradation products of full-length TRN-1. The left-hand blot is a western blot of recombinant wild-type TRN-1 protein. Individual bands from 2 independent preparations were quantified using Image J and the relative abundance of TRN-1 is provided as mean values \pm SD.



Extended Data Fig. 7 | see figure caption on next page.

Extended Data Fig. 7 | Fate of CA and TRN-1 after translocation through the NPC. a, Arresting cells in G1/S does not alter HIV-1 dependency on TRN-1. P4 cells were infected with VSVG pseudotyped HIV-1 in the presence of 8 μ M Aphidicolin (APH) or DMSO as control. β -gal activity was measured at 2 dpt. Results are the mean of 3 independent experiments performed in triplicate \pm s.e.m. ns=0.5346 and 0.2381 for shTRN-1 and shTNR-3, respectively. Cell cycle arrest in G1/S was confirmed by propidium iodide labelling and flow cytometry (right panel). **b,** TRN-1 and CA co-localize in the nucleus of target cells at 8 h.p.i. HeLa cells transduced with EC or shTRN-1 eGFP lentiviral vectors, were infected with HIV-1-VSVG or left uninfected. Duolink labelling was performed using anti-rabbit TRN-1 and anti-mouse p24, and image stacks were acquired using a LSM880 confocal microscope. Scale bar = 10 μ M. The nuclear volume and CA spots within 0.3 μ m distance of the nuclear envelope were detected in 3D using Imaris. Quantification was performed on 3 different stacks and shown as mean \pm SD. Images are representative of 2 independent experiments. **c,** TRN-1 relocates to the nucleus in infected cells at 24 h.p.i. HeLa cells were infected with HIV-1-VSVG or left uninfected, and labelled with anti-TRN-1 antibody at 24 h.p.i. Scale bar = 10 μ M. Mean grey intensity values in the cytoplasm and nuclei were quantified for each cell using Fiji on n nuclei from 4 separate acquisitions (mean values \pm s.e.m.). **** $p < 0.0001$. Results are representative of 2 independent experiments.

Reporting Summary

Nature Research wishes to improve the reproducibility of the work that we publish. This form provides structure for consistency and transparency in reporting. For further information on Nature Research policies, see [Authors & Referees](#) and the [Editorial Policy Checklist](#).

Statistical parameters

When statistical analyses are reported, confirm that the following items are present in the relevant location (e.g. figure legend, table legend, main text, or Methods section).

n/a | Confirmed

- The exact sample size (n) for each experimental group/condition, given as a discrete number and unit of measurement
- An indication of whether measurements were taken from distinct samples or whether the same sample was measured repeatedly
- The statistical test(s) used AND whether they are one- or two-sided
Only common tests should be described solely by name; describe more complex techniques in the Methods section.
- A description of all covariates tested
- A description of any assumptions or corrections, such as tests of normality and adjustment for multiple comparisons
- A full description of the statistics including central tendency (e.g. means) or other basic estimates (e.g. regression coefficient) AND variation (e.g. standard deviation) or associated estimates of uncertainty (e.g. confidence intervals)
- For null hypothesis testing, the test statistic (e.g. F , t , r) with confidence intervals, effect sizes, degrees of freedom and P value noted
Give P values as exact values whenever suitable.
- For Bayesian analysis, information on the choice of priors and Markov chain Monte Carlo settings
- For hierarchical and complex designs, identification of the appropriate level for tests and full reporting of outcomes
- Estimates of effect sizes (e.g. Cohen's d , Pearson's r), indicating how they were calculated
- Clearly defined error bars
State explicitly what error bars represent (e.g. SD, SE, CI)

Our web collection on [statistics for biologists](#) may be useful.

Software and code

Policy information about [availability of computer code](#)

Data collection CellQuest (BD), Image Lab 5.1 (Biorad), Magellan (Tecan), NanoWizard® 4 NanoScience AFM (JPK Instruments, Brucker)

Data analysis Image Lab 5.1 (Bio-Rad), GraphPadPrism 6, Serial Cloner, FlowJo 10.0.8r (LLC), ImageJ, Imaris

For manuscripts utilizing custom algorithms or software that are central to the research but not yet described in published literature, software must be made available to editors/reviewers upon request. We strongly encourage code deposition in a community repository (e.g. GitHub). See the Nature Research [guidelines for submitting code & software](#) for further information.

Data

Policy information about [availability of data](#)

All manuscripts must include a [data availability statement](#). This statement should provide the following information, where applicable:

- Accession codes, unique identifiers, or web links for publicly available datasets
- A list of figures that have associated raw data
- A description of any restrictions on data availability

All unique materials used are readily available from the authors or from standard commercial sources.

Field-specific reporting

Please select the best fit for your research. If you are not sure, read the appropriate sections before making your selection.

Life sciences Behavioural & social sciences Ecological, evolutionary & environmental sciences

For a reference copy of the document with all sections, see [nature.com/authors/policies/ReportingSummary-flat.pdf](https://www.nature.com/authors/policies/ReportingSummary-flat.pdf)

Life sciences study design

All studies must disclose on these points even when the disclosure is negative.

Sample size	No statistical analysis was used to determine sample size
Data exclusions	All experiments with validated inputs (equal protein expression, or validated knock-down) were included in the analysis
Replication	Replication attempts were successful
Randomization	Experiments did not involve randomisation
Blinding	Confocal microscopy experiments represent blinded acquisitions

Reporting for specific materials, systems and methods

Materials & experimental systems

n/a	Included in the study
<input type="checkbox"/>	<input checked="" type="checkbox"/> Unique biological materials
<input type="checkbox"/>	<input checked="" type="checkbox"/> Antibodies
<input type="checkbox"/>	<input checked="" type="checkbox"/> Eukaryotic cell lines
<input checked="" type="checkbox"/>	<input type="checkbox"/> Palaeontology
<input checked="" type="checkbox"/>	<input type="checkbox"/> Animals and other organisms
<input checked="" type="checkbox"/>	<input type="checkbox"/> Human research participants

Methods

n/a	Included in the study
<input checked="" type="checkbox"/>	<input type="checkbox"/> ChIP-seq
<input type="checkbox"/>	<input checked="" type="checkbox"/> Flow cytometry
<input checked="" type="checkbox"/>	<input type="checkbox"/> MRI-based neuroimaging

Unique biological materials

Policy information about [availability of materials](#)

Obtaining unique materials Blood samples from healthy donors were obtained from EFS (Paris and Toulouse) to isolate CD4+ T lymphocytes.

Antibodies

Antibodies used

Mouse Anti-βactin clone AC-15 (Sigma A1978) - 1/3000
 Rabbit Anti-Alpha Tubulin clone DM1A (Sigma 9026) - 1/3000
 Mouse Anti-Lamin A/C (Leica NCL-LAM-A/C) - 1/200
 Rabbit Anti-CypA C-14-R (Santa Cruz sc-20360-R) – 1/250
 Rat anti-HA clone 3F10 (Roche 11867423001) – 1/1000
 Mouse anti-HA clone HA-7 (Sigma H3663 – 1/500
 Rabbit anti-HA (Abcam ab9110) – 1/20 000
 Mouse anti-Flag clone M2 (Sigma F3165) – 1/20000
 Mouse anti-P24 clone 183-H12-5C (NIH Reagent Program 3537) – 1/1000
 Mouse anti-P24 clone AG3.0 (NIH Reagent Program 4221) – 1/1000
 Rabbit anti-P24 clone SF2 (NIH Reagent Program 4250) – 1/1000
 Mouse anti-Integrase IN-2 kindly provided by Marc Lavigne
 Mouse anti-TRN-1 clone D45 (Abcam ab10303) – 1/1000
 Mouse anti-KPNB1 clone H7 (Santa Cruz sc-137016) – 1/500
 Mouse anti-TNPO3 (Abcam ab54353) – 1/500
 Mouse anti-Karyophérine β3 (IPO5) clone H-4 (Santa Cruz sc-17802) – 1/500
 Mouse anti-IPO7 H-12 (Santa Cruz sc-271701) – 1/1000
 Goat anti-mouse-HRP (GE Healthcare NA931VS) – 1/3000

Goat anti-rabbit-HRP (GE Healthcare NA934VS) – 1/3000
 Goat anti-rat-HRP (Abcam ab97057) – 1/20 000
 Rabbit anti-goat-HRP (BD Serotec Star 122p) – 1/2000
 Goat anti-rabbit A647 (Molecular Probes) – 1/1000
 Goat anti-mouse A647 (Molecular Probes A21237) – 1/1000
 Goat anti-mouse A488 (Life Tech A-11029) – 1/1000
 Goat anti-rabbit A488 (Life Tech A-11034) – 1/1000
 Mouse anti-human HLA-DR-FITC clone L243 (BD 347401)
 Mouse anti-human CD1a-PE clone SK9 (BD 333167)
 Mouse anti-human CD14-APC clone TÚK4 (Miltenyi 130-098-070)
 Mouse anti-human CD11c-FITC clone 3.9 (eBiosciences 11-0116-41)
 Mouse anti-human CD4-APC clone S3.5 (Caltag MHC-D0405)
 Mouse anti-human CD86-PE clone BU63 (Caltag MHC-D8604)
 Mouse anti-human CD209-FITC clone DCN46 (BD 561765)
 Mouse CD3-PE clone 10D12 (Miltenyi 130-092-009)

Validation

Each antibody was used according to the manufacturer's instruction

Eukaryotic cell lines

Policy information about [cell lines](#)

Cell line source(s)

P4 cells were obtained from the NIH AIDS Reagent Program (Ref. 120)
 P4.R5 cells MAGI were obtained from Nathaniel Landau
 HeLa ATCC HeLa (ATCC® CCL2™) lot 63226283
 HEK 293T ATCC 293T/17 [HEK 293T/17] (ATCC® CRL11268™)

Authentication

Cell lines were authenticated by the ATCC or NIH AIDS Reagent Program

Mycoplasma contamination

All ATCC cell lines were tested for mycoplasma contamination. P4 cells were tested for mycoplasma using VenorGeM One-step mycoplasma detection kit (Minerva Biolabs) and results was negative.

Commonly misidentified lines
(See [ICLAC](#) register)

Name any commonly misidentified cell lines used in the study and provide a rationale for their use.

Flow Cytometry

Plots

Confirm that:

- The axis labels state the marker and fluorochrome used (e.g. CD4-FITC).
- The axis scales are clearly visible. Include numbers along axes only for bottom left plot of group (a 'group' is an analysis of identical markers).
- All plots are contour plots with outliers or pseudocolor plots.
- A numerical value for number of cells or percentage (with statistics) is provided.

Methodology

Sample preparation

cells are washed once in PBS and fixed in 2% PFA for at least 10min before acquisition

Instrument

Acquisition were performed using FACS CALIBUR from Becton Dickinson company

Software

CellQuest (BD) software was used for acquisition and FlowJo 10.0.8r (LLC) for data analysis

Cell population abundance

Flow cytometry experiments performed in cell lines show a unique population of living cells, representing more than 90% of the total sample.

Gating strategy

Preliminary FSC/SSC gate was placed around the unique cell population to remove dead cells and debris, and representing more than 90% of the total cells in the sample. Then, using the negative control without secondary anti-body, or non-GFP expression, a gate was place at the right of the cell population FSC/marker, which would then represent positive cells.

- Tick this box to confirm that a figure exemplifying the gating strategy is provided in the Supplementary Information.